(2)

MEMORANDUM REPORT BRL-MR-3857

BRL

DIRECT NUMERICAL SIMULATION OF TURBULENT COUETTE FLOW, PART II

JOHN D. KUZAN
PHILLIP C. DYKSTRA

AUGUST 1990

U.S. ARMY LABORATORY COMMAND

BALLISTIC RESEARCH LABORATORY
ABERDEEN PROVING GROUND, MARYLAND

Original contains color plates: All DTIC reproductions will be in black and white

NOTICES

Destroy this report when it is no longer needed. DO NOT return it to the originator.

Additional copies of this report may be obtained from the National Technical Information Service, U.S. Department of Commerce, 5285 Port Royal Road, Springfield, VA 22161.

The findings of this report are not to be construed as an official Department of the Army position, unless so designated by other authorized documents.

The use of trade names or manufacturers' names in this report does not constitute indorsement of any commercial product.

REPORT DOCUMENTATION PAGE

Form Approved
OMB No. 0704-0188

1. AGENCY USE ONLY (Leave blank)	2. REPORT DATE	3. REPORT TYPE AND DATES COVERED
	August 1990	Final, Dec 89 - Jun 90

4. TITLE AND SUBTITLE
Direct Numerical Simulation of Turbulent Couette Flow, Part II

5. FUNDING NUMBERS
1L161102AH43

6. AUTHOR(S)
John D. Kuzan and Phillip C. Dykstra

7. PERFORMING ORGANIZATION NAME(S) AND ADDRESS(ES)

8. PERFORMING ORGANIZATION REPORT NUMBER

9. SPONSORING/MONITORING AGENCY NAME(S) AND ADDRESS(ES)
Ballistic Research Laboratory
ATTN: SLCBR-DD-T
Aberdeen Proving Ground, MD 21005-5066

10. SPONSORING/MONITORING AGENCY REPORT NUMBER
BRL-MR-3857

11. SUPPLEMENTARY NOTES
Part I of this report, entitled "Direct Numerical Simulation of Turbulent Couette Flow," was published as a BRL Memorandum Report, BRL-MR-3848, dated June 1990.

12a. DISTRIBUTION/AVAILABILITY STATEMENT
Approved for public release; distribution is unlimited.

12b. DISTRIBUTION CODE

13. ABSTRACT (Maximum 200 words)

A direct simulation of fully developed turbulent channel flow has been performed, through a direct solution of the time-varying, incompressible, Navier-Stokes equations. Reynolds shear stress appears to mark structures that are similar to those marked by hydrogen bubbles in the near-wall region of wall bounded shear flows. This has been observed by others, but not from animated views that match closely the physical experiments. Three-dimensional views of the Reynolds shear stress reveal elongated structures in the near-wall region that do not appear to be connected at larger normal distances.

14. SUBJECT TERMS
Projectiles, Turbulence
Base Flow, Simulation

15. NUMBER OF PAGES
49

16. PRICE CODE

17. SECURITY CLASSIFICATION OF REPORT	18. SECURITY CLASSIFICATION OF THIS PAGE	19. SECURITY CLASSIFICATION OF ABSTRACT	20. LIMITATION OF ABSTRACT
UNCLASSIFIED	UNCLASSIFIED	UNCLASSIFIED	SAR

INTENTIONALLY LEFT BLANK.

TABLE OF CONTENTS

INTENTIONALLY LEFT BLANK.

List of Figures

INTENTIONALLY LEFT BLANK.

1 Introduction

In a previous report[1], direct numerical simulation of turbulent fluid flow between two parallel flat plates was described, and the results of tests that showed the close match between the simulation and nature were presented. This report examines the flow field in more detail.

The direct simulation is accomplished by solving the equations governing the motion of an incompressible fluid, which are the Navier-Stokes equations:

$$\frac{\partial \mathbf{v}}{\partial t} = -\mathbf{v}\cdot\nabla\mathbf{v} - \frac{1}{\rho}\nabla p + \nu\nabla^2\mathbf{v} \tag{1}$$

and the continuity equation:

$$\nabla\cdot\mathbf{v} = 0. \tag{2}$$

In these equations, $\mathbf{v}$ is the instantaneous three dimensional velocity vector, t is the time, ρ is the density of the fluid, p is the hydrodynamic pressure, and ν is the kinematic viscosity. Here the coordinate system is Cartesian, and (x, y, z) are directions streamwise, normal to the flat plates, and spanwise with corresponding velocity components (u, v, w).

Velocity and length are made dimensionless in this report with the kinematic viscosity, ν, and the skin-friction velocity, u^*:

$$u^+ = \frac{u}{u^*} \qquad x^+ = \frac{u^*}{\nu}x. \tag{3}$$

In this numerical study, the dimensionless distance between the flat plates was 300 viscous units to give a Reynolds number of 2260 (a pipe Reynolds number of approximately 8,000). The Reynolds number is $\frac{u_b h}{\nu}$ where u_b is the streamwise bulk velocity, and was 13.8 in viscous units.

If the instantaneous velocity vector is replaced in Equations 1 and 2 with a velocity vector that is decomposed into a mean flow, $\mathbf{V}$, and a fluctuating velocity, $\tilde{\mathbf{v}}$, such that:

$$\mathbf{v} = \mathbf{V} + \tilde{\mathbf{v}} \tag{4}$$

then the resulting "Reynolds-decomposed" Navier-Stokes equations contain an additional tensor called the Reynolds stress tensor. This report focuses on one part of this tensor, the Reynolds shear stress, $\tilde{u}\tilde{v}$ (see Figure 1), and its relation to the production of turbulence.

2 Description of Wall Bounded Turbulence

Work in the direct simulation of wall turbulence has produced a description of events, although a theory for wall turbulence is at least a few years away. The central problem is to determine how velocity fluctuations (fluid turbulence) are generated and sustained [2]. Thus, the question to be answered is: how is energy transferred from the pressure gradient to the velocity fluctuations? In an effort to answer this, Hanratty [2] developed

the picture first presented by Townsend [3]. Hanratty suggests that near wall eddies, with their rotational axis aligned in the streamwise direction, have inflows and outflows that are of the same strength and that, in a time-averaged sense, the in- and outflows are coupled. The eddies create streamwise velocity fluctuations by bringing low momentum fluid from the wall into the outer flow. The opposite is also true; *i.e.*, they carry high momentum fluid toward the wall. High momentum fluid is transported by negative (toward the wall) normal velocities; low momentum fluid is transported by positive normal velocities. Hence, with this transfer process, when the normal velocity is positive, the fluctuating streamwise velocity is negative. This means that both in- and outflows are associated with values of the Reynolds shear stress that are negative.

For flow between two flat plates, the production of turbulent kinetic energy is given by:

$$\kappa = -\overline{\tilde{u}^+\tilde{v}^+}\frac{dU^+}{dy^+} \tag{5}$$

where κ is the production term and U^+ is the average streamwise velocity. Thus, production of turbulent kinetic energy, in an instantaneous sense, is the product of negative Reynolds shear stress and the mean velocity gradient. Figure 2 shows the time-averaged Reynolds shear stress and the production of turbulent kinetic energy versus distance from the wall. The region of significant turbulence production is between 5 and 45 viscous units away from the wall, and is a maximum near 12 viscous units from the wall. The Reynolds shear stress is a maximum near 30 viscous units from the wall.

3 Results

3.1 Distribution of Reynolds Shear Stress

Figure 1 shows a simple view of the Reynolds shear stress and its contribution to the production of turbulent kinetic energy. The fluctuating normal velocity is displayed on the ordinate and the fluctuating streamwise velocity on the abscissa; the resulting plot shows the four "quadrants" of the Reynolds shear stress. Reynolds shear stress in the first and third quadrants reduces the production of turbulent kinetic energy; the second and fourth quadrants contribute to the turbulent kinetic energy. This quadrature is helpful in the analysis of some of the following figures.

The distribution of Reynolds shear stress among the quadrants varies with distance from the wall, and this is shown in Figures 3 through 10. Also shown in the figures is the fraction of the Reynolds shear stress contributed by values of $\tilde{u}\tilde{v}$ lower than some "threshold" value. The threshold varies from zero to four in the figures because the Reynolds shear stress is made dimensionless with the square of the friction velocity. The values along the ordinate are normalized with the total Reynolds shear stress; hence, for a threshold level of zero, the total stress has a value of one.

Figure 3 shows the distribution at 1.62 units from the wall, where most of the Reynolds shear stress comes from quadrant 4 events. At 8.77 units from the wall (Figure 4), slightly

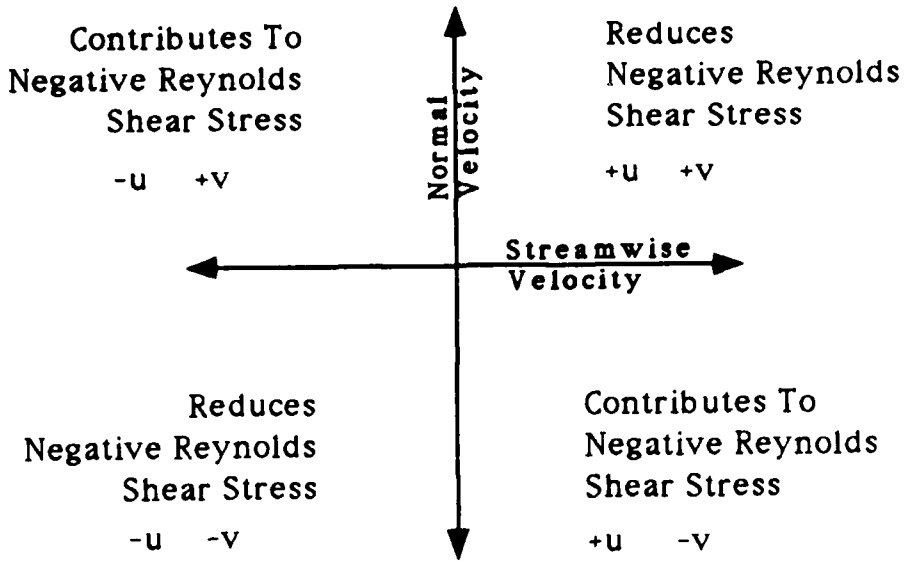

Figure 1: Reynolds Shear Stress Quadrature

more than half of the Reynolds shear stress is above a threshold of one. Quadrant 4 events still dominate, although quadrant 2 events are significant.

Where the production of turbulence is a maximum, $y^+ = 11.4$ (Figure 5), quadrants 2 and 4 are roughly equal in their contribution, which is 120% of the total. Quadrants 1 and 3 effectively remove the excess 20%. Now, more than three quarters of the Reynolds shear stress is above the threshold of one. At a location near the maximum Reynolds stress, $y^+ = 17.7$ (Figure 6), the levels within quadrants 2 and 4 have reversed, although their total is similar to the location where the production was a maximum. Almost 90% of the Reynolds shear stress is above the threshold of one.

The remaining plots of the Reynolds shear stress distribution are not in the region of significant turbulence production, but are of some interest none-the-less. Figure 7 shows that quadrant 2 Reynolds shear stress dominates at $y^+ = 38.8$, while quadrant 4 is still large. Ninety-five per cent of the Reynolds shear stress is above the threshold of one. The next two figures, Figures 8 and 9, show the percentage of Reynolds shear stress above a threshold of one decreasing as the distance from the wall increases. Figure 10 shows the distribution half way between the flat plates. In this location there is confusion between positive and negative normal velocities because what is positive for one wall is negative for the other. The Reynolds shear stress is almost zero; the resulting quadrature plot is not too informative, other than showing that the total Reynolds shear stress has 60% of its contribution above the threshold of one.

3.2 Instantaneous Velocities In Two Dimensions

The figures in this section are two-dimensional views of velocity vectors in either the streamwise-normal or spanwise-normal directions. Vectors in the figures have a velocity unit length of 10 viscous units of distance. Only a small section of the flow field is shown (typically one quarter of the full two-dimensional view that would be available) so that some detail can be seen.

The first figure in this section, Figure 11, shows a full cross-section of the flow field; the bulk flow is into the page. About two-thirds of the velocity vectors have been removed so that the resulting plot is not a blur of ink. Along a constant value of 150 in the normal direction there are three distinct large-scale events at spanwise distances of about 200, 700, and 900; these are marked with large circles on the plot. At 200, there is a strong flow toward the top wall (the top wall is at $y^+ = 300$); at 900 there is flow in the opposite direction. Near 700, the flowfield appears to be a point source of fluid. Along both walls there appear to be many counter-rotating eddies. At the wall, the velocity vectors alternate direction every 50 units or so. This is consistent with experiments that have characterized the spanwise spacing of the eddies [4].

At the top wall and in the spanwise direction at 125 there is a strong flow toward the wall, or an "inflow." Again at the top wall and at 325 there is a strong "outflow." These two events are marked with large squares on the plot. In these two events, the fluctuating streamwise velocity is such that large values of Reynolds shear stress are produced; the proximity to the wall insures that the velocity gradient is large and hence the turbulence production is large, also (see Equation 5). The next two figures (Figures 12 and 13) expand the inflow and outflow; also the wall is shown at the bottom of the plot so that y^+ values are meaningful and up is positive in the normal direction.

The inflow in Figure 12 is clear at a value of approximately 120; the flow appears to penetrate the wall (this is an illusion) suggesting a strong negative normal velocity. On either side of the inflow, the spanwise velocity is directed away from the inflow. The center of one eddy appears to be at a value of 140 in the spanwise (z^+) direction and 15 in the normal direction. Its associated eddy has a center near $z^+ = 95$ (hence, it is centered on the inflow with respect to the spanwise direction), but it is lifted away from the wall to a value of about 25. Typically, in- and outflows are not centered between two eddies; this will be more clear in the next figure. The location of the center is somewhat confused by the motion of the fluid above the eddy. There are outflows at z^+ values of 60 and 155; another inflow is at $z^+ = 225$. Thus the spacing of about 100 units between in- and outflows is found in this small portion of the cross-section.

Figure 13 shows the outflow at a spanwise distance of about 320. On either side of the outflow, the spanwise velocity is directed toward the outflow. The center of one eddy (the "right-hand side") is located near $y^+ = 22$ and $z^+ = 335$; this eddy appears egg-shaped, and it has a diameter of about 50 units on its long axis and 25 units in the spanwise direction. Its associated eddy (the "left-hand side") is located a long distance from the wall near $y^+ = 50$ and $z^+ = 280$, and its diameter is over 100 units. Lyons [5] has shown that typical

eddy pairs consist of two eddys of different size, as is found in the pair just described. Furthermore, the interaction of the eddies with one another (and the surrounding fluid) causes the eddies to lift away from the wall. Beneath the eddy on the left-hand side of the outflow in Figure 13 fluid is moving in the direction opposite the circulation of the eddy (the region is encircled on the figure). In some sense, this is similar to a separated flow. As fluid is entrained in the reverse flow (near $z^+ = 270, y^+ = 10$), the separated region grows in size and is lifted from the wall. This is shown in Figure 14, which is about 30 units downstream. The region is encircled in this figure, also. Note that the centers of both the left-hand and right-hand eddies have moved farther from the wall. Going back to Figure 13, it is possible that the eddy with center located at $z^+ = 410, y^+ = 30$ was at one time paired with the eddy on the left-hand side of the outflow. In a process similar to the growth of the separated region just described, the right-hand side eddy may have been spawned and in that process the original eddies were lifted away from the wall. To this end, note the small separated regions along the wall at $z^+ = 360$ and 450.

The next three figures show streamwise-normal views of the flow field that are centered on the inflow in the streamwise direction. The bulk flow is in the positive streamwise direction. Figure 16 is centered on the inflow in the spanwise direction, while Figure 15 is about 7 units to the left and Figure 17 is 7 units to the right of the inflow. As shown in all three figures, the fluctuating streamwise velocity is strong and positive in the vicinity of $y^+ = 11$; this coupled with the strong negative normal velocity of the inflow produces large negative Reynolds shear stress, and that gives a high value to the turbulence production. Between streamwise values of 200 and 380, there is an organized structure that appears to be attached to the wall and rises to about $y^+ = 20$. These structures are common in all streamwise-normal views of the flowfield and suggest the process of lifting the eddies off the wall that was described above. Figure 18 is an expanded view of Figure 16. Here the inflow with its associated large streamwise velocity is somewhat more clear.

Figures 19 through 21 are similar to the three figures described in the paragraph above; these three are centered on the outflow. Here, positive normal velocities are associated with negative streamwise velocities giving large values of the turbulence production. Once again structures appear attached to the wall and lifted into the outer flow downstream, although in this case the associated streamwise velocities are negative.

3.3 Instantaneous Reynolds Shear Stress In Two Dimensions

A threshold value of 1.0 for the magnitude of the Reynolds shear stress was used to produce the figures in this section. The first three figures show Reynolds shear stress above the threshold in the same cross-sectional view of the flow field as Figure 11. Figure 22 shows velocity vectors for all quadrant 2 Reynolds shear stress above a threshold of 1.0; Figure 23 shows quadrant 4; and Figure 24 shows both quadrant 1 and 3. Note the approximate spanwise spacing of 100 units for the quadrant 2 and 4 Reynolds shear stress. Quadrants 1 and 3 have few events where the stress is above the threshold. In the center of the flowfield at $y^+ = 150$, there is some confusion in the sign of the Reynolds shear stress because the

definition of positive and negative changes depending on which wall is being considered. For this reason, several quadrant 1 and 3 events appear to come from nowhere near the center; similarly some quadrant 2 and 4 events disappear.

Of more interest are streamwise-spanwise views of the instantaneous fluctuating velocities in that plane, with color used to distinguish between the quadrants. Figures 25 through 31 show these views at the normal distances that were used to produce Figures 3 through 9. Since the normal velocities are somewhat arbitrary in the center of the channel, the Reynolds shear stress at $y^+ = 144$ is not presented. In these figures, Reynolds shear stress above a threshold dimensionless stress of 1.0 is colored: yellow for quadrants 1 and 3, blue for quadrant 2, and red for quadrant 4. Green is used for stress below the threshold. Due to the resolution of the media used to print the color pictures, individual velocity vectors are not discernable. None-the-less, streaky structures are clear in the pictures. In the figures, the origin is in the lower left hand corner, the streamwise distance increases to the right and the spanwise distance increases toward the top of the page. This is shown in the small schematic on each page.

Figure 25 contians no stress above the threshold level, although there is an indication of the streaky structures shown in the next figure. At $y^+ = 8.77$, a large portion of the stress above the threshold is in the fourth quadrant; this is consistant with Figure 4. The streaks of red and blue appear next to one another frequently. These streaks resemble the streaks found in hydrogen bubble experiments [4]. In these experiments, a bubble wire was stretched in the spanwise direction across the wall in a water tunnel and was positioned at various heights above the wall. Streaks of bubbles would form in the streamwise direction, suggesting the near-wall counter-rotating eddies that pump fluid from the wall to the outer flow and vice versa. These streaky structures were evenly spaced at about 100 viscous units. Lyons [5] showed streaky structures in Reynolds shear stress, also.

Figure 27 is at $y^+ = 11.4$, where the production of turbulence is a maximum. Again, the streaky structures are clear. The spanwise spacing of approximately 100 units is maintained. At a larger normal distance (Figure 28), the streaks tend to broaden. The quadrant 1 and 3 events appear to be much more fan-like and do not form streaks. Figure 29 shows the steaky structures begining to break up and either become less elongated or curl up. Again, this is consistant with hydrogen bubble experiments. At this distance, second quadrant stress dominates fourth quadrant stress.

At $y^+ = 66.6$ (Figure 30), the streaky structures have almost disappeared and the stress appears as blobs of color. Quadrant 1 and 3 stress is now significant. It continues to be significant in the next figure, Figure 31, where there is little quadrant four stress.

3.4 Instantaneous Reynolds Shear Stress In Three Dimensions

Unfortunately, three-dimensional views do not reproduce well, nor is it possible to show the animated views that were produced using the data from the simulation.

Three-dimensional views of Reynolds shear stress were produced by coloring three-dimensional regions in the flow field where the stress was above some threshold (usually

1.0). These views showed the shape of iso-surfaces of Reynolds shear stress and suggested that the streaks were not connected at large values of normal distance. Efforts to visualize hairpin-like structures in Reynolds shear stress were unsuccessful.

Time-varying velocity vectors colored with Reynolds shear stress above a certain threshold were animated in two-dimensions to produce, for example, a time-varying streamwise-spanwise view at a constant normal distance. These studies showed streaky structures of Reynolds shear stress that followed closely the motions of hydrogen bubbles in wall bounded shearflow.

4 Conclusions

Reynolds shear stress appears to mark structures that are similar to those marked by hydrogen bubbles in the near-wall region of wall bounded shear flows. This is been observed by others, but not from animated views that match closely the physical experiments. Further study should concentrate on describing the motion of the streaky structures. Three-dimensional views of the Reynolds shear stress reveal elongated structures in the near-wall region that do not appear to be connected at larger normal distances.

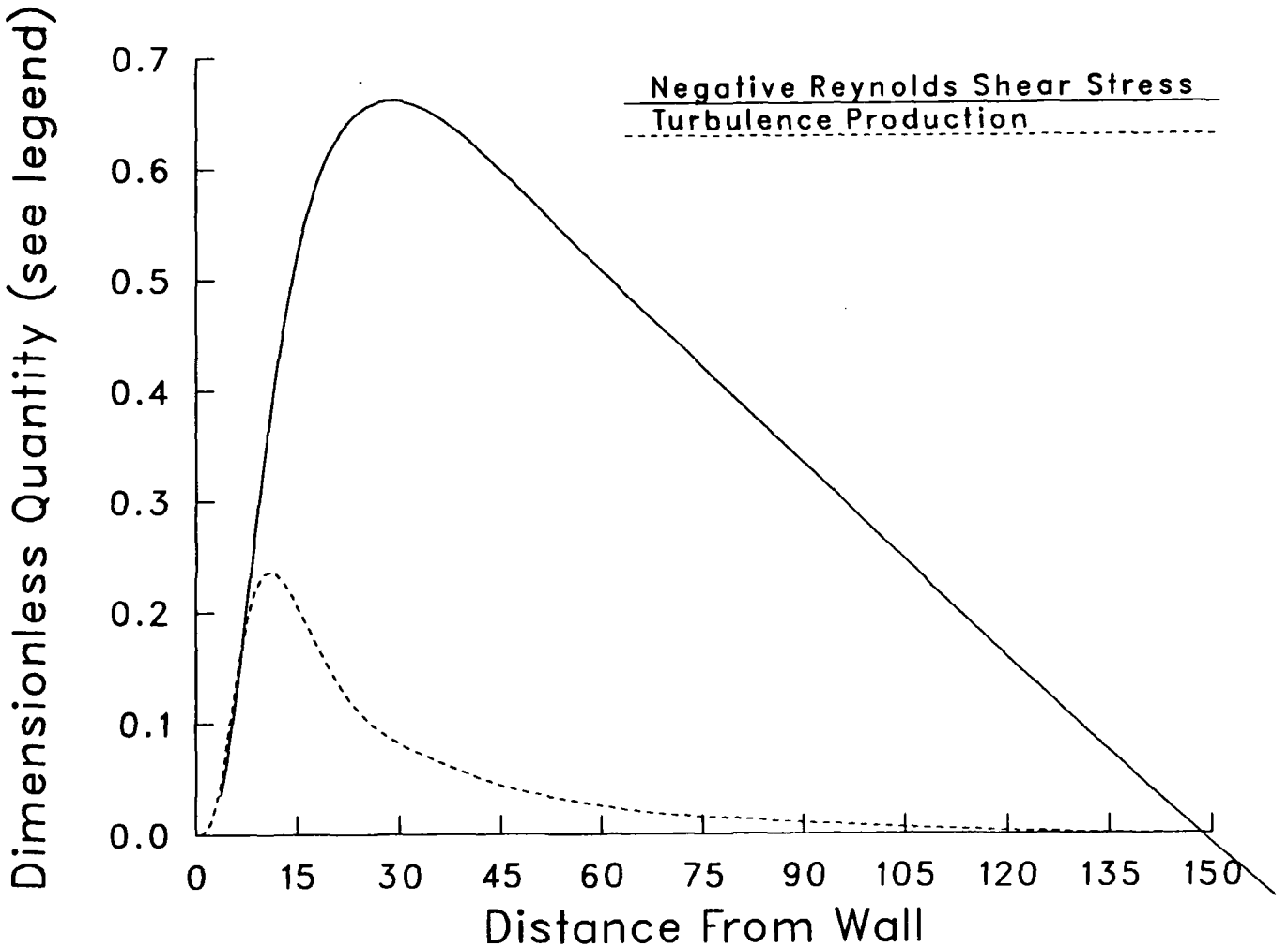

Figure 2: Reynolds Shear Stress and Turbulent Energy Production

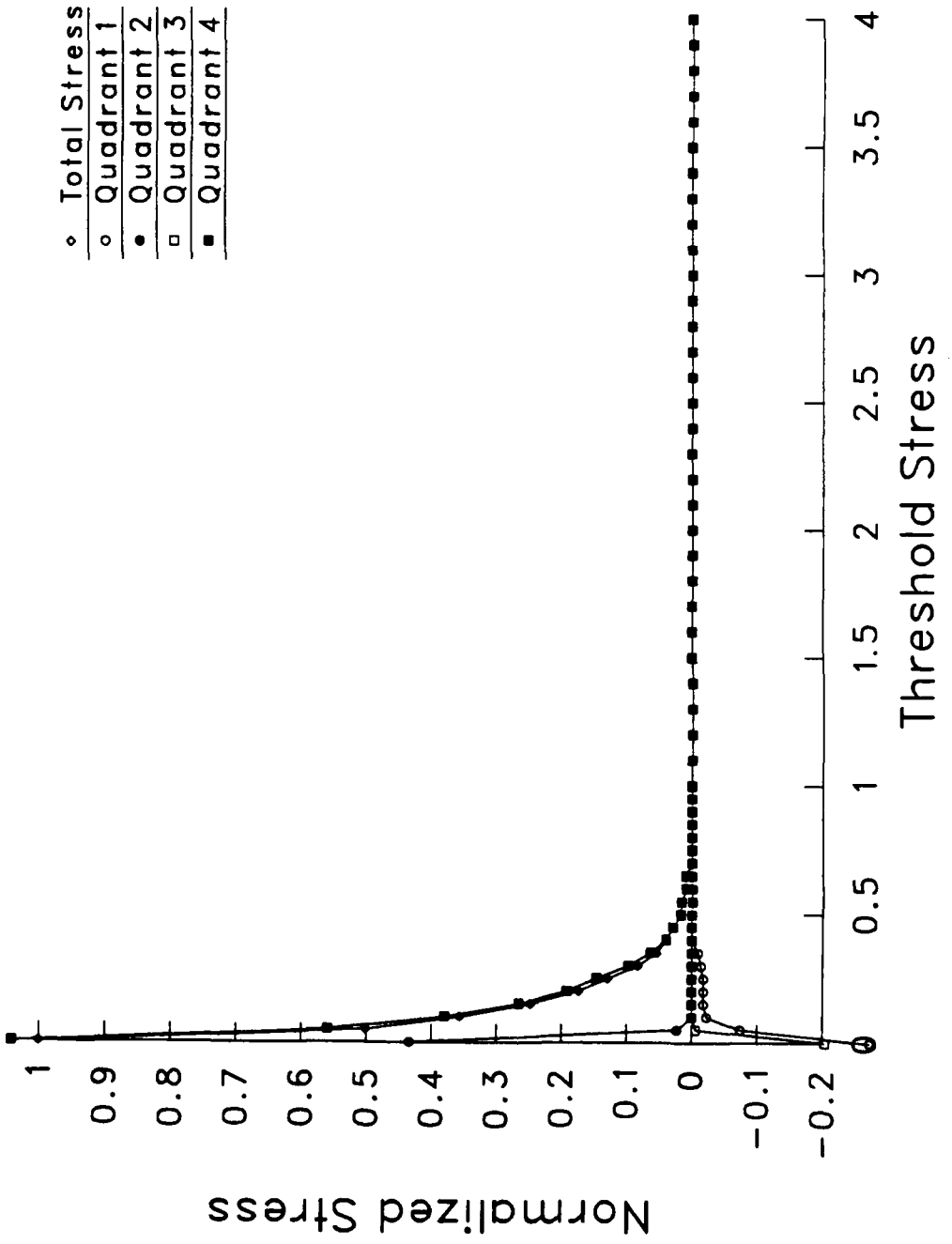

Figure 3: Reynolds Shear Stress Distribution, $y^+ = 1.62$

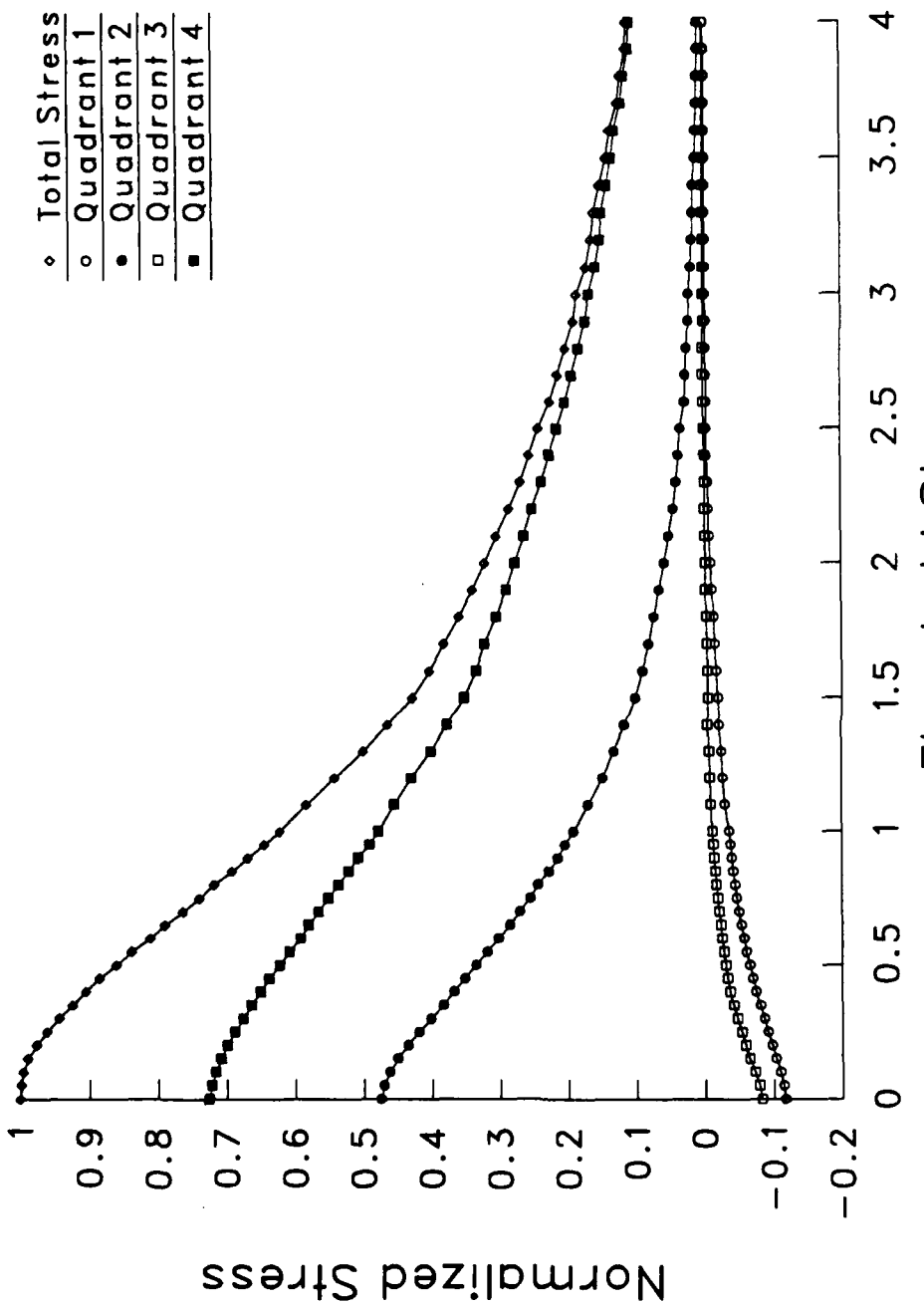

Figure 4: Reynolds Shear Stress Distribution, $y^+ = 8.77$

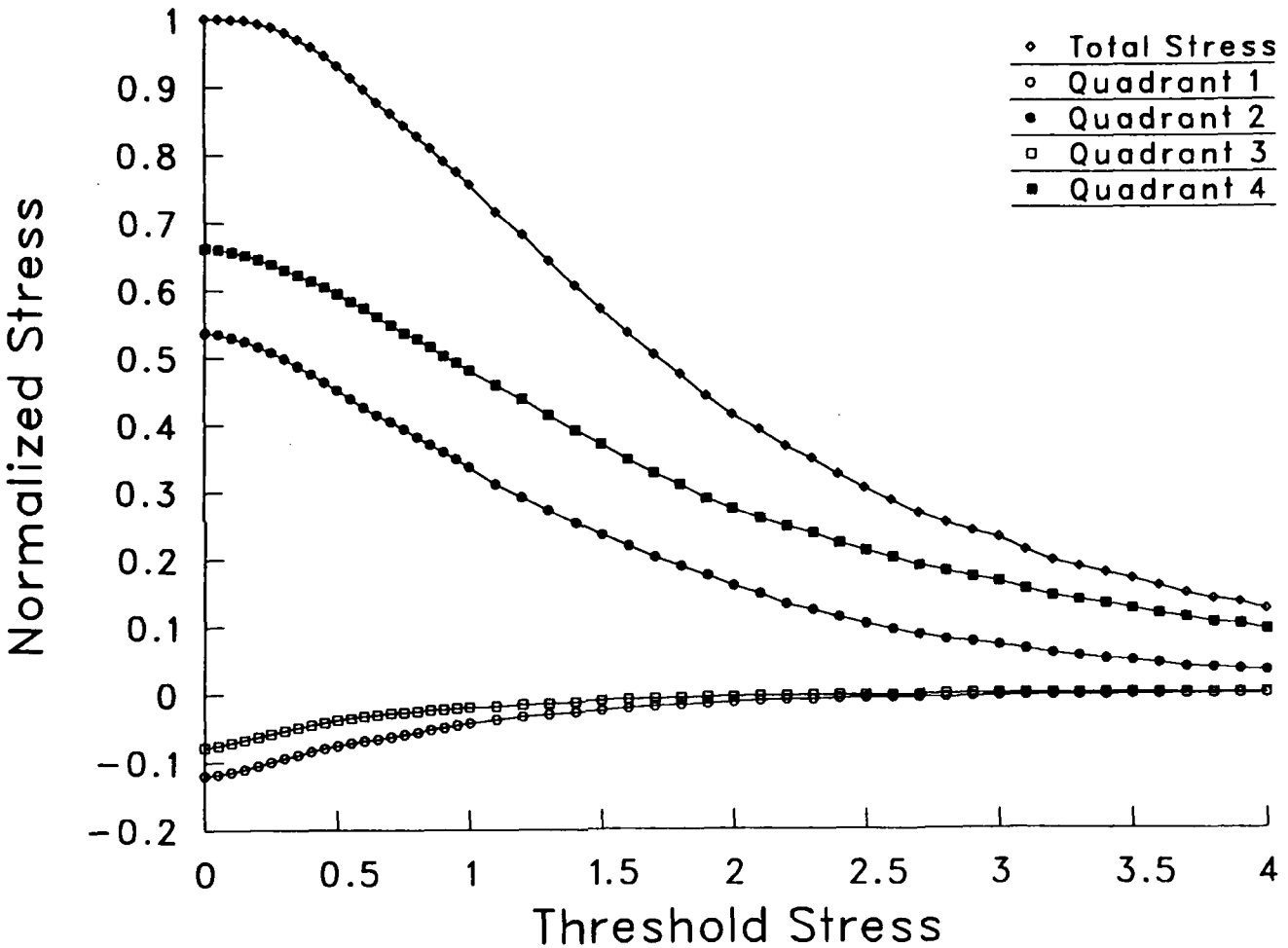

Figure 5: Reynolds Shear Stress Distribution, $y^+ = 11.4$

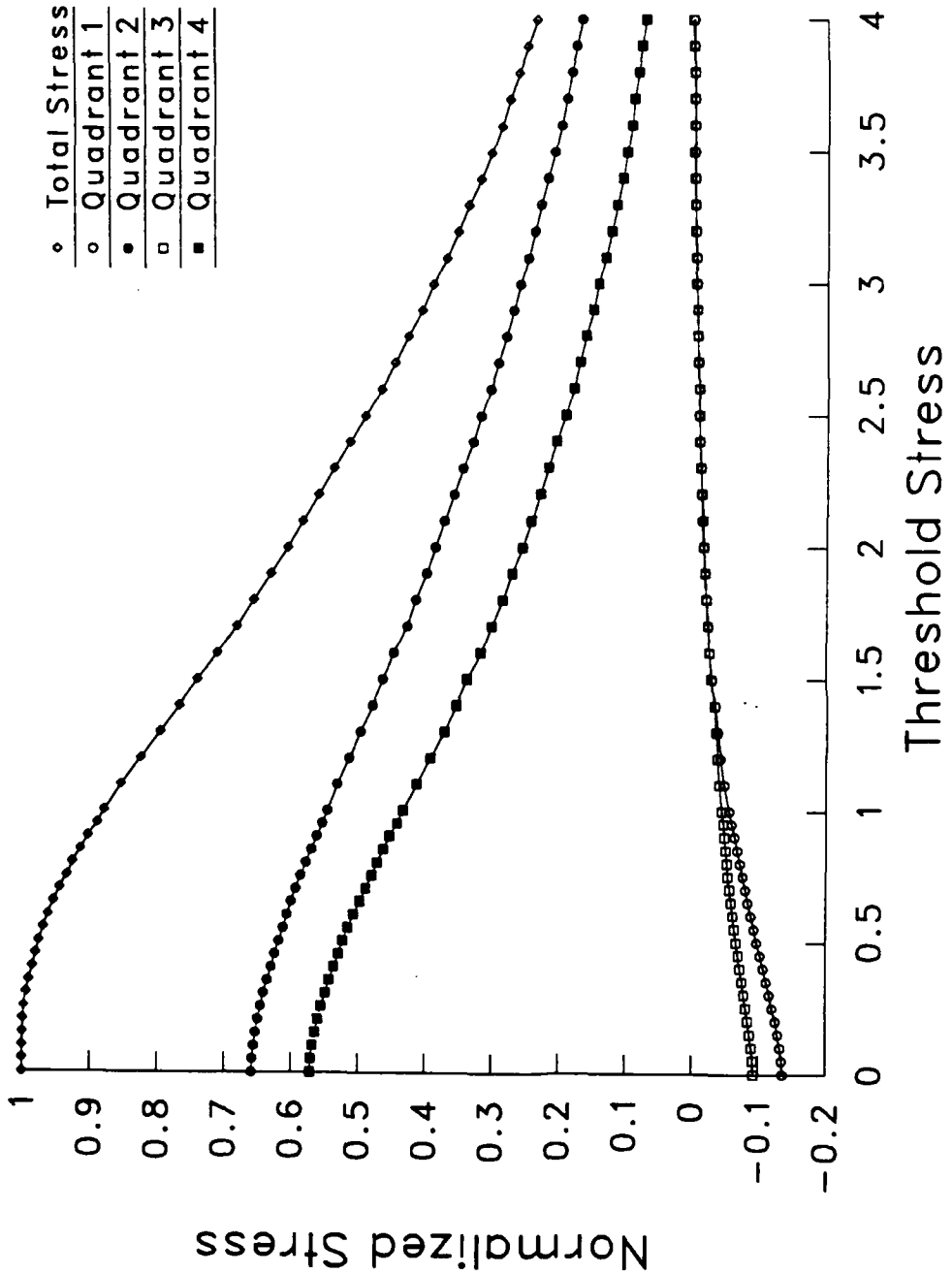

Figure 6: Reynolds Shear Stress Distribution, $y^+ = 17.7$

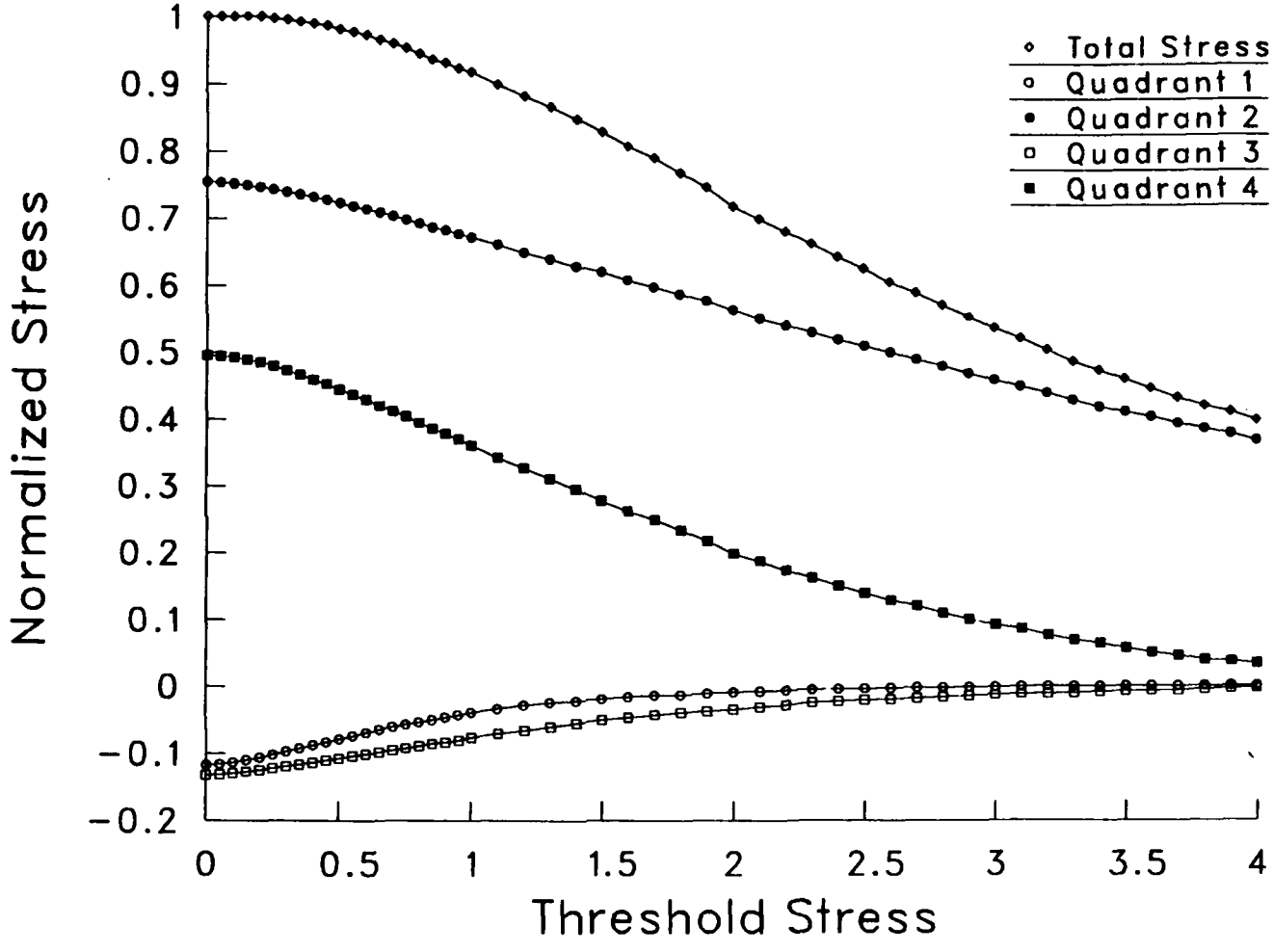

Figure 7: Reynolds Shear Stress Distribution, $y^+ = 38.8$

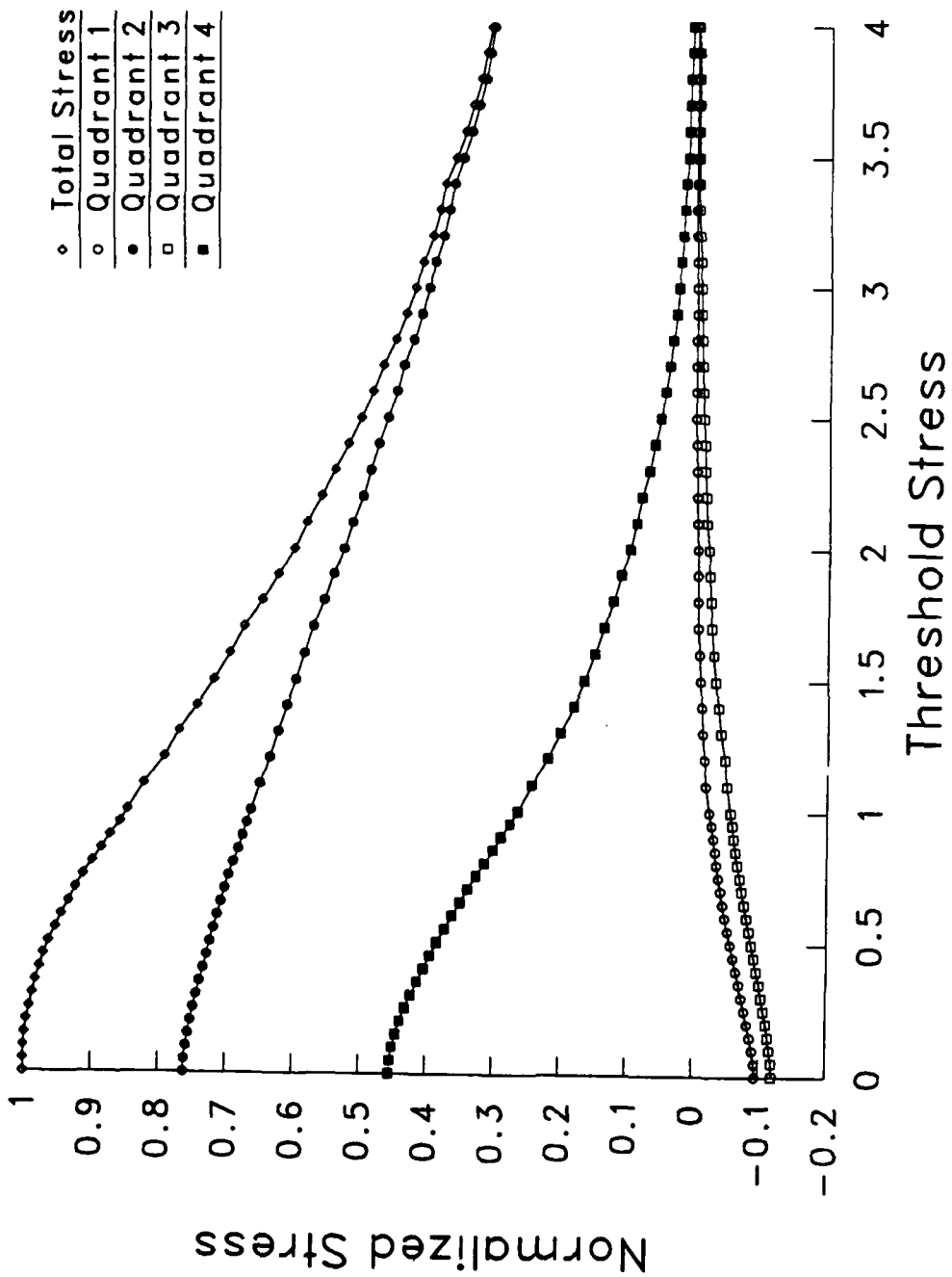

Figure 8: Reynolds Shear Stress Distribution, $y^+ = 66.6$

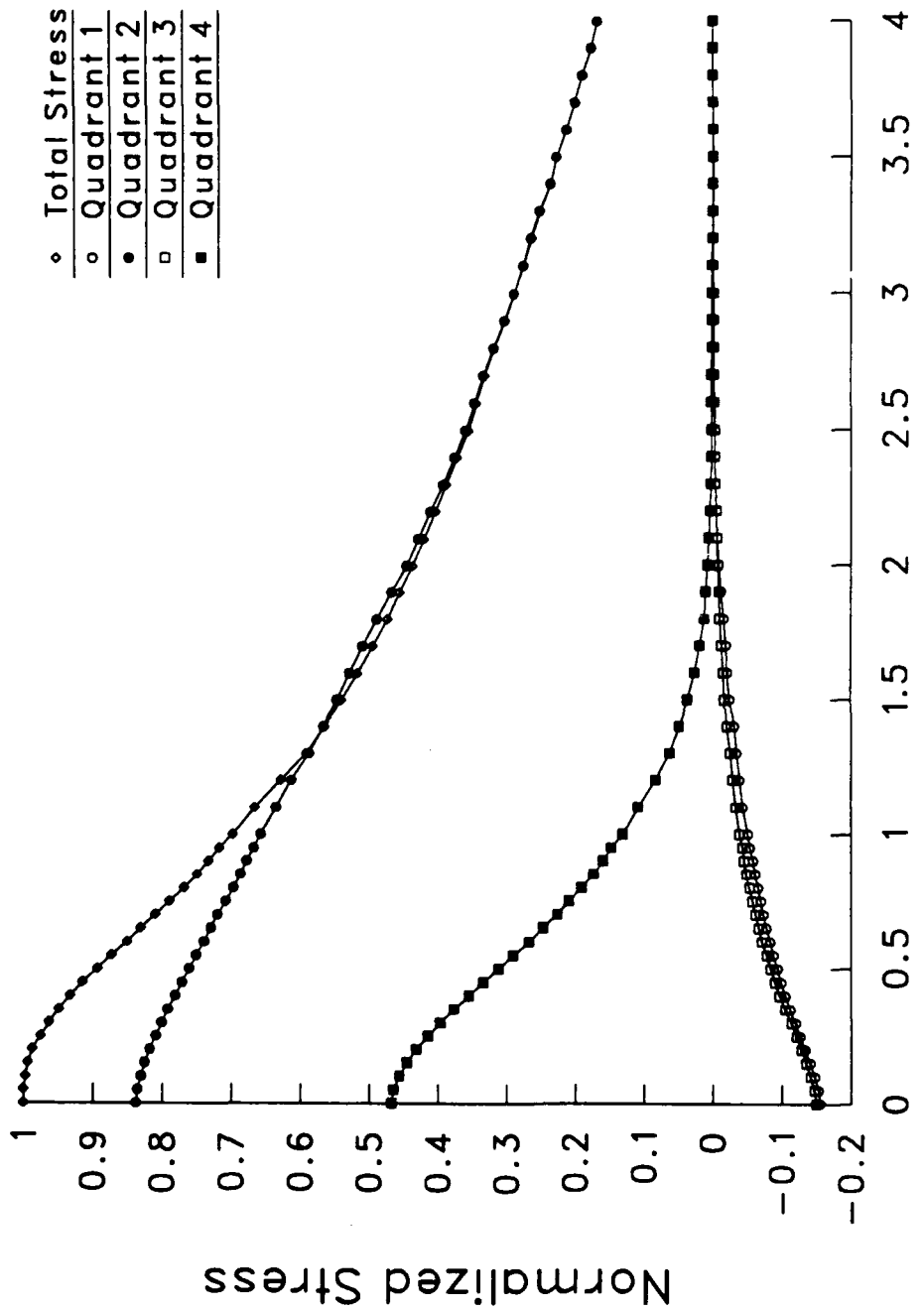

Figure 9: Reynolds Shear Stress Distribution, $y^+ = 99.5$

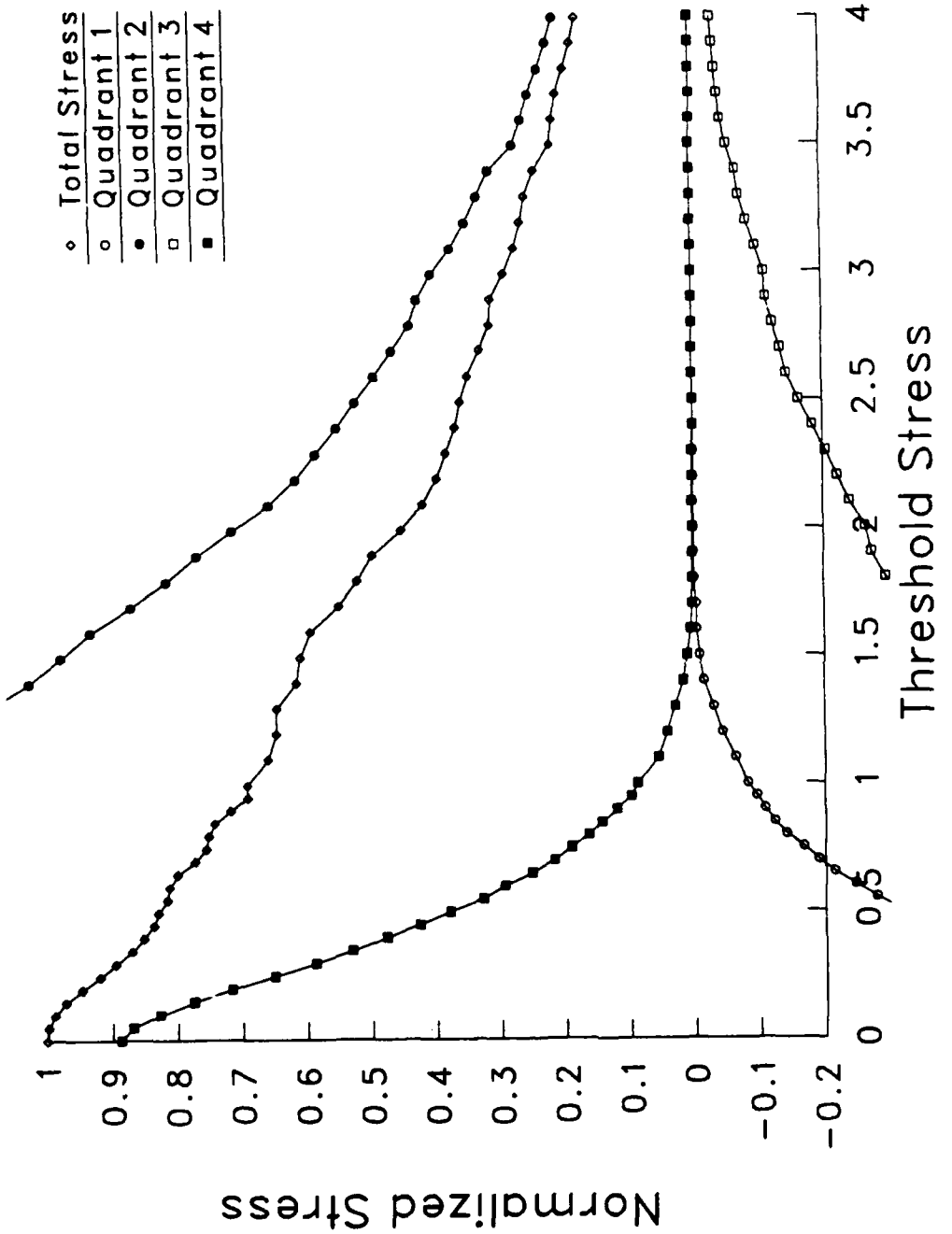

Figure 10: Reynolds Shear Stress Distribution, $y^+ = 144.3$

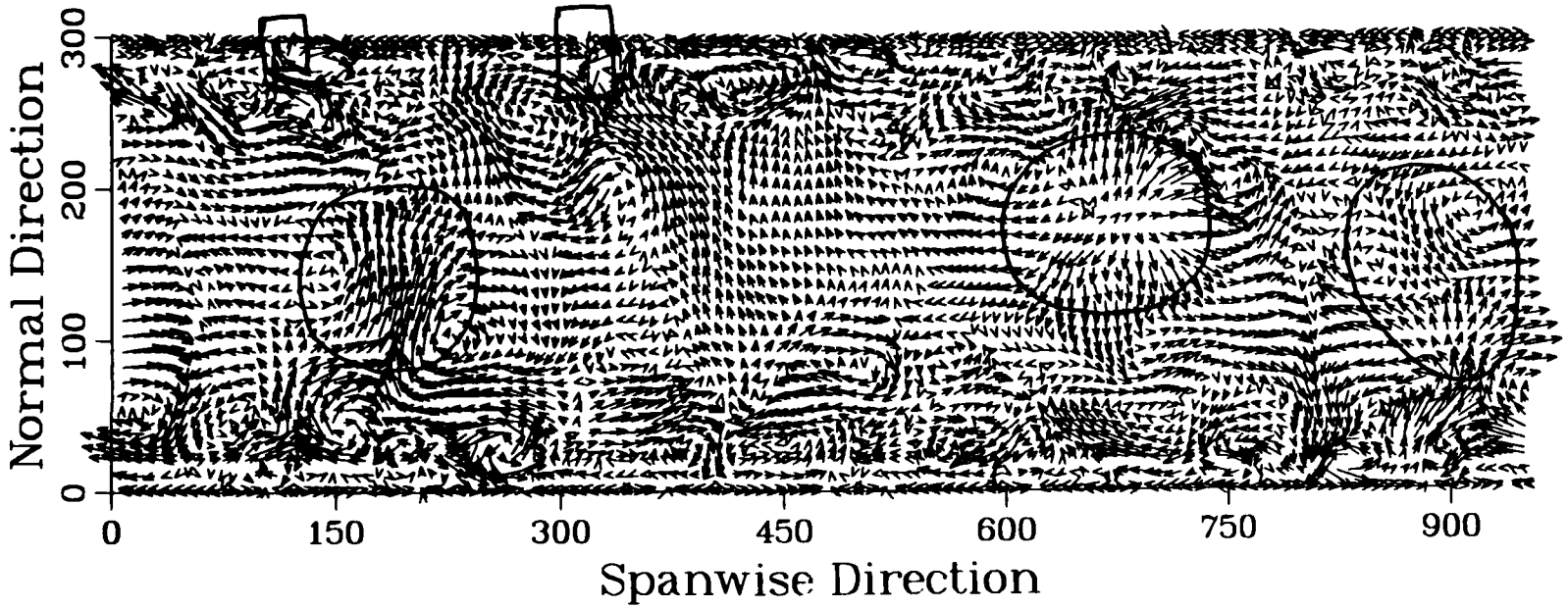

Figure 11: Full Spanwise-Normal View of Instantaneous Velocity Vectors

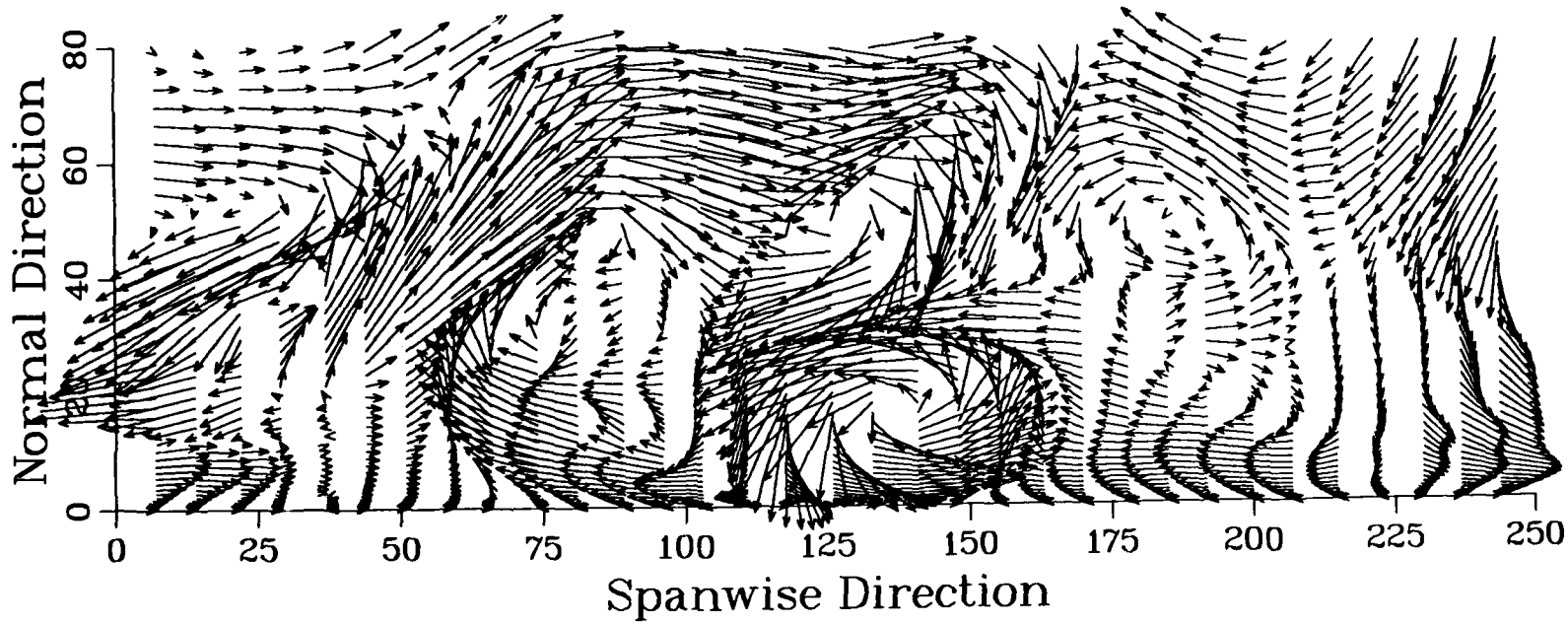

Figure 12: Spanwise-Normal View of an Inflow

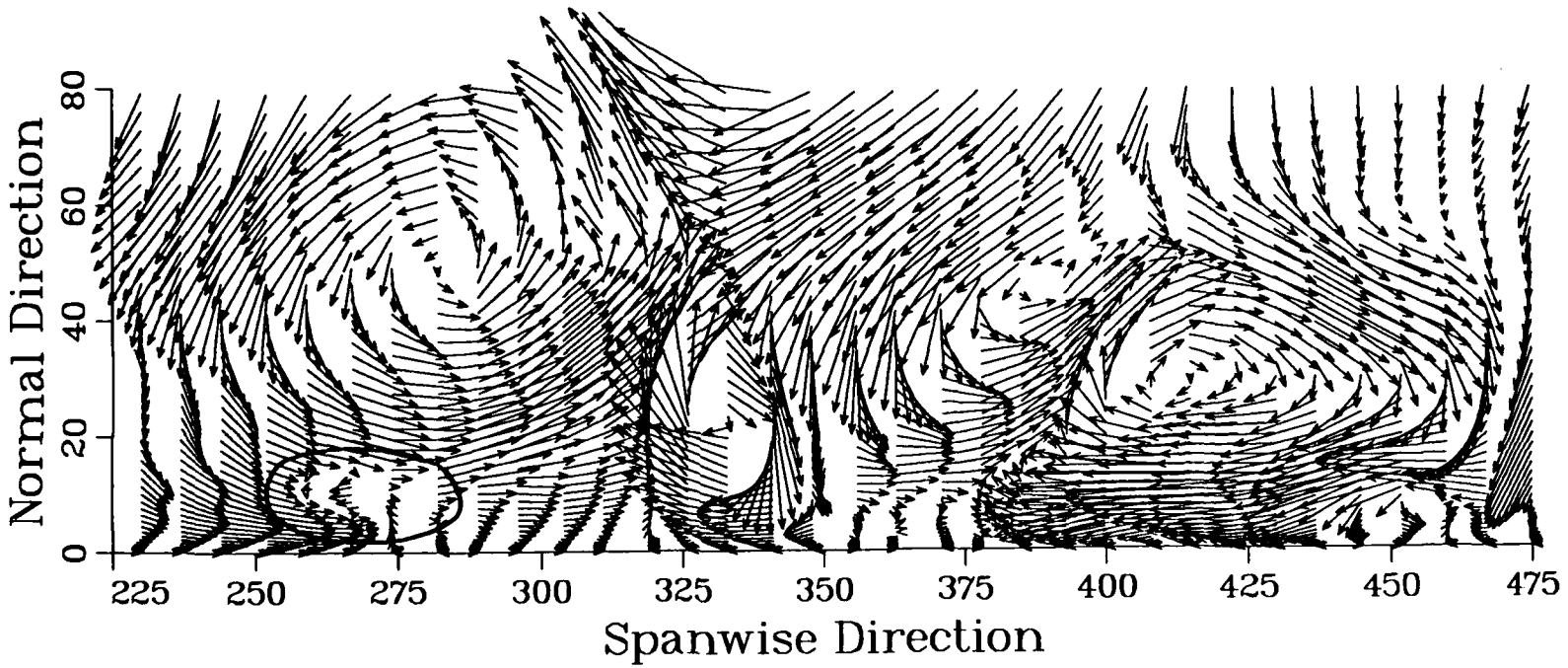

Figure 13: Spanwise-Normal View of an Outflow

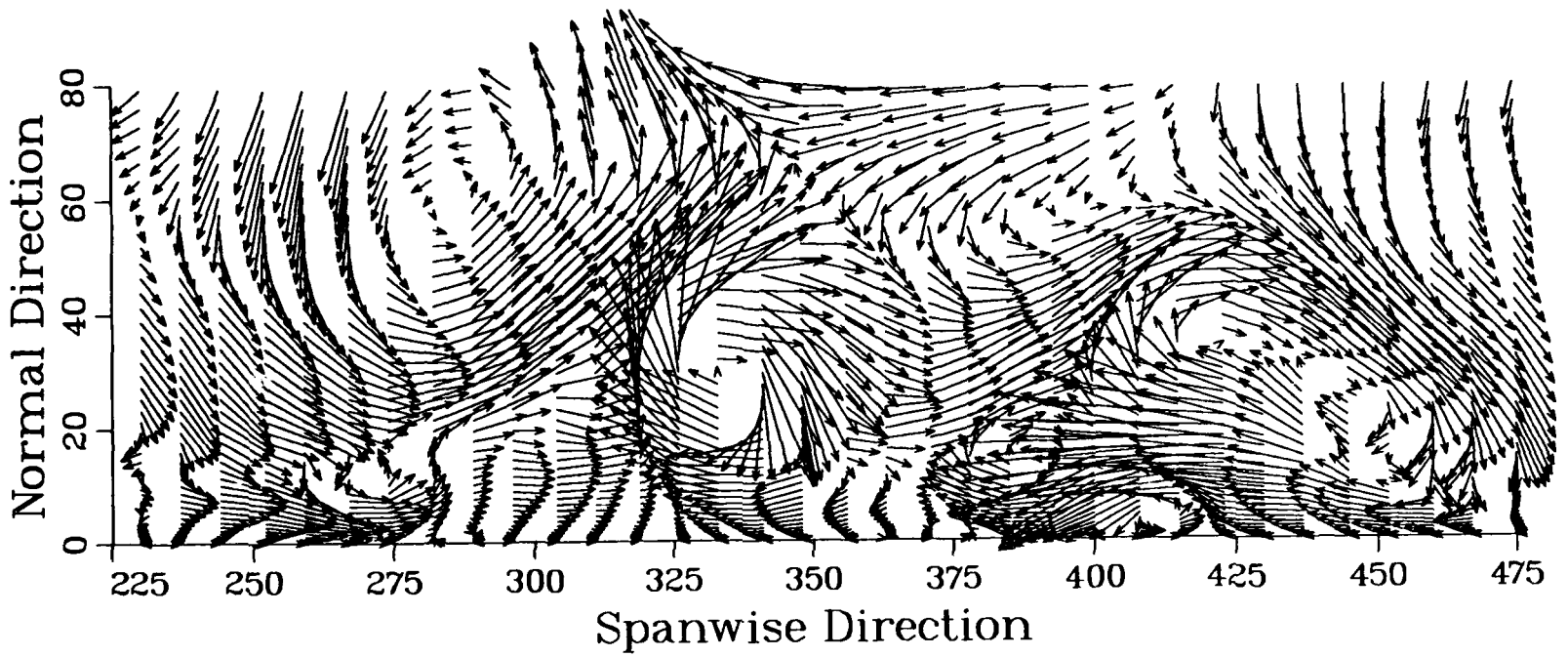

Figure 14: Spanwise-Normal View of an Outflow; Downstream of Main Flow

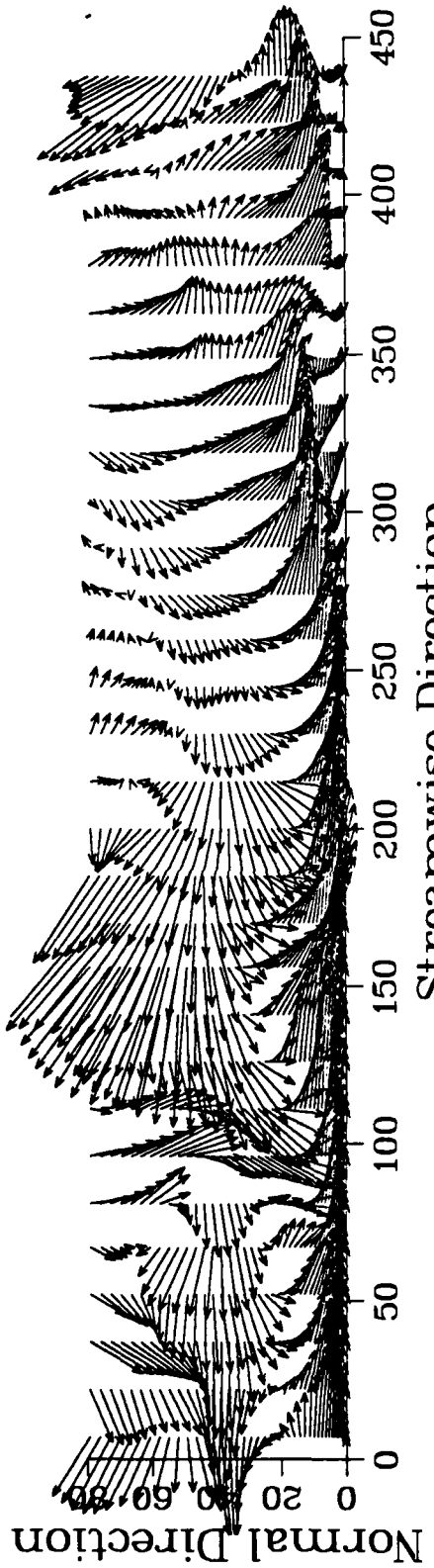

Figure 15: Streamwise-Normal View of an Inflow; Left Side

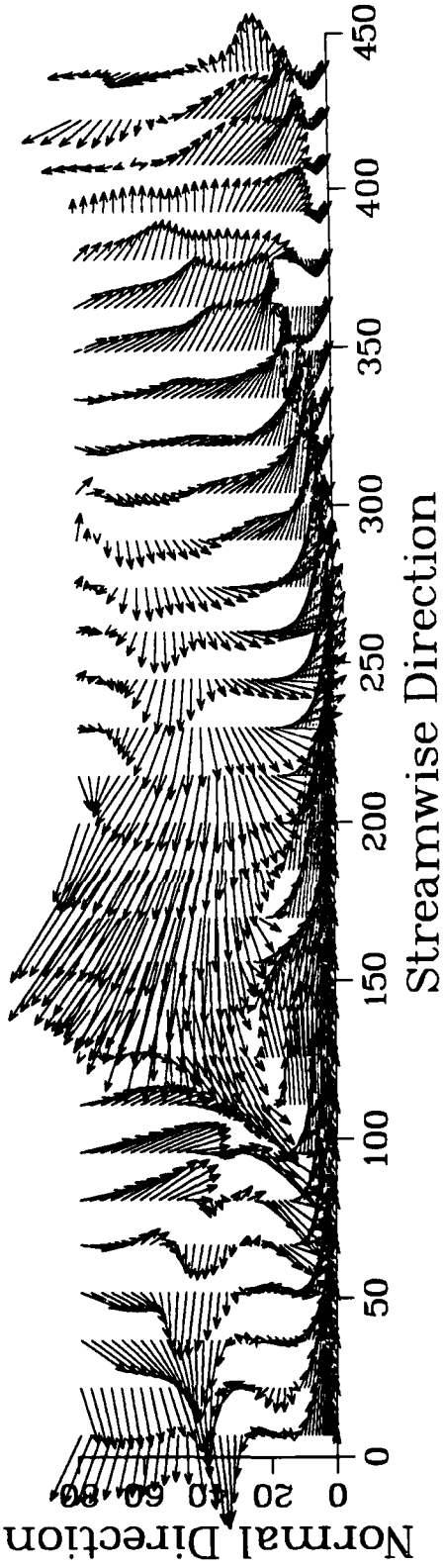

Figure 16: Streamwise-Normal View of an Inflow; Center

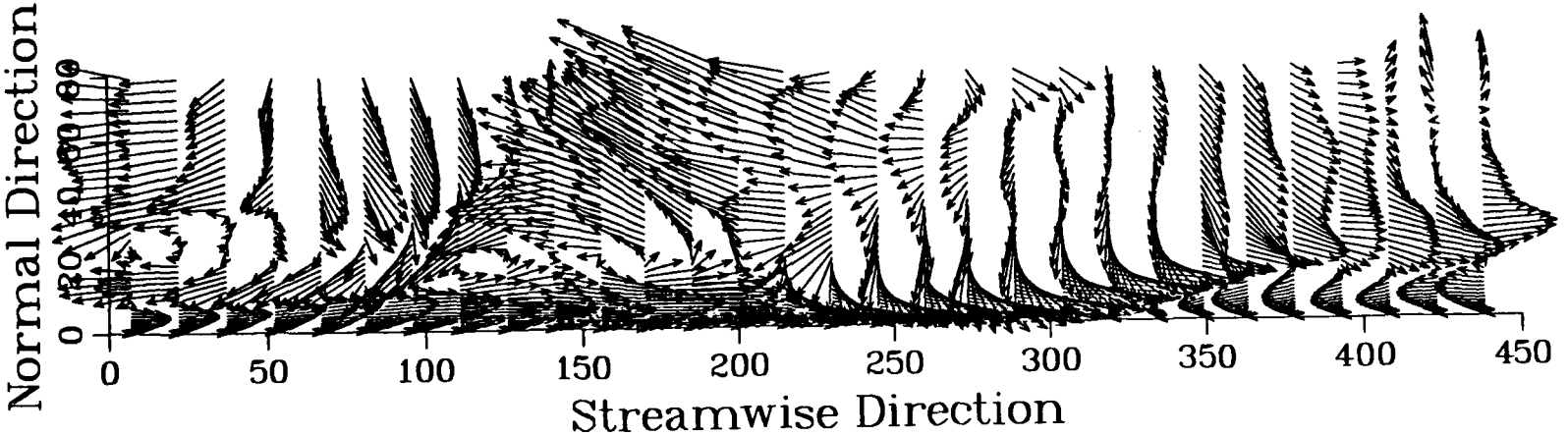

Figure 17: Streamwise-Normal View of an Inflow; Right Side

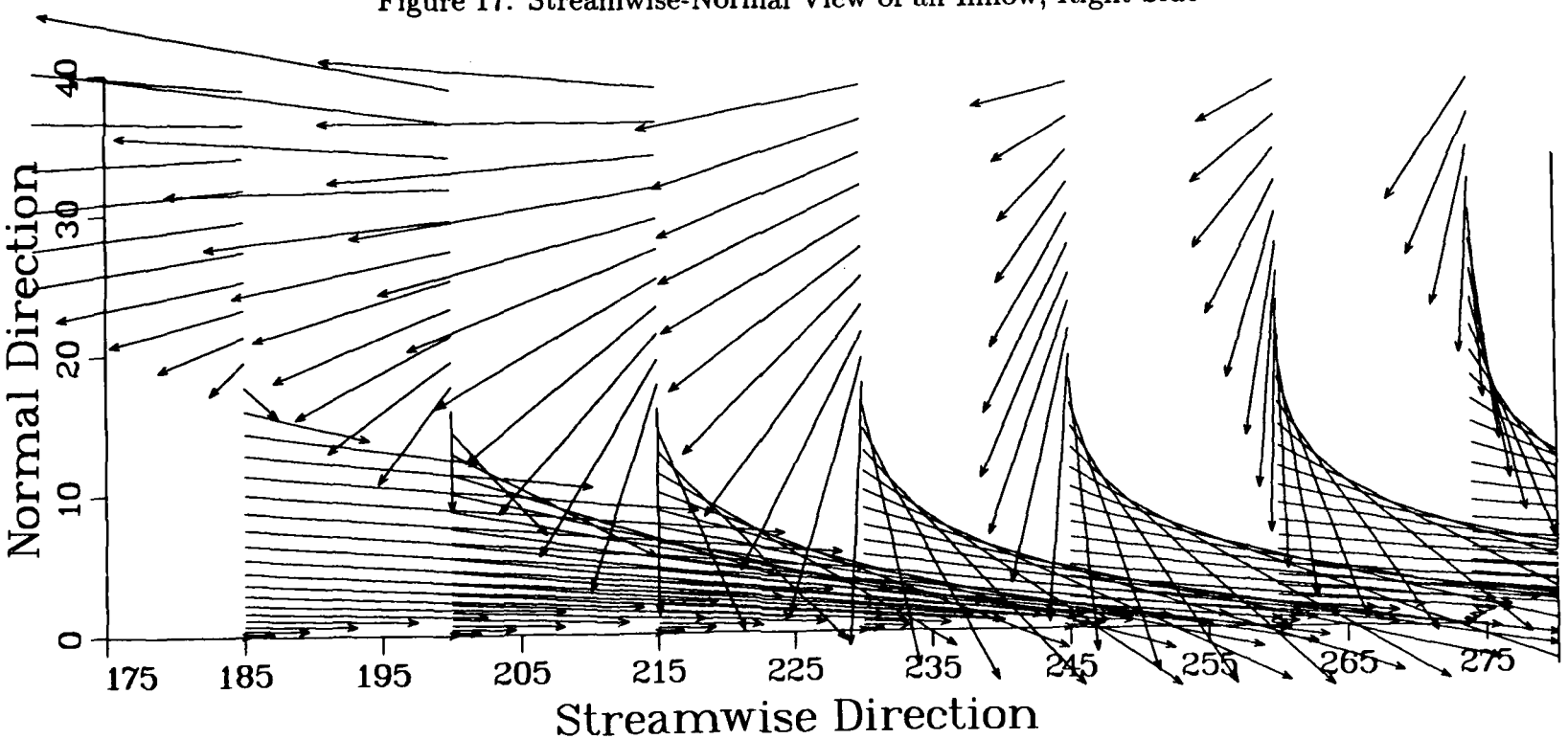

Figure 18: Streamwise-Normal View of an Inflow; Expanded View

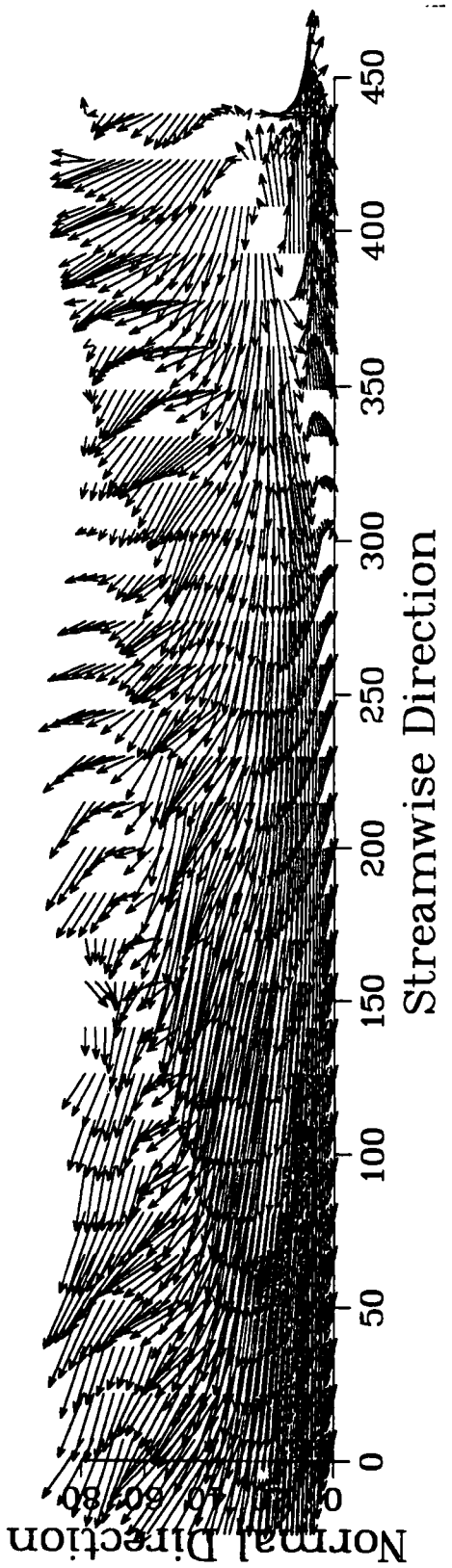

Figure 19: Streamwise-Normal View of an Outflow; Left Side

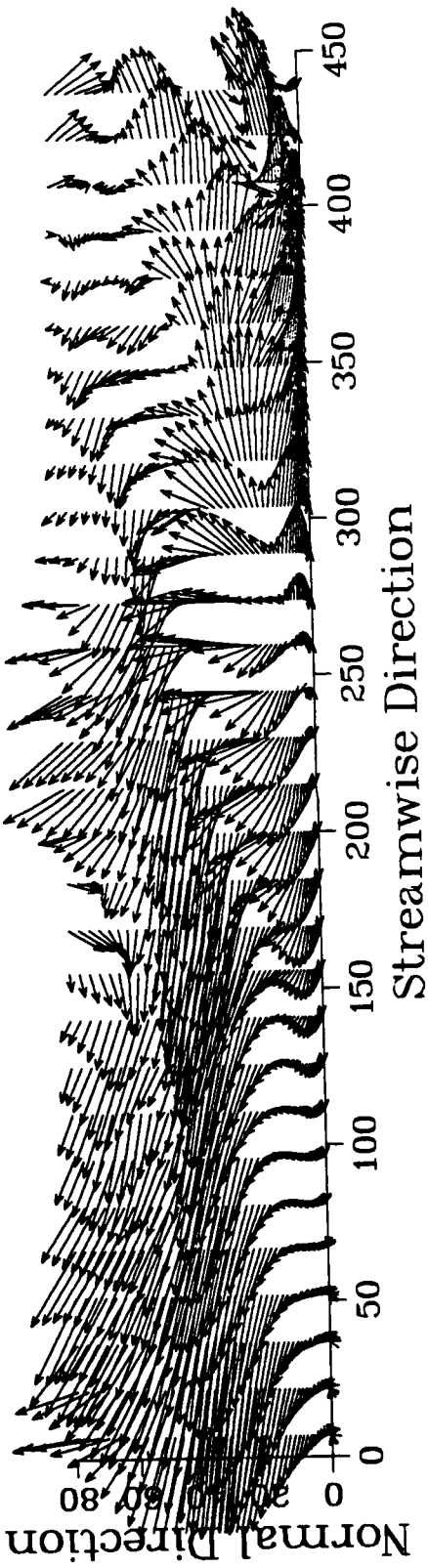

Figure 20: Streamwise-Normal View of an Outflow; Center

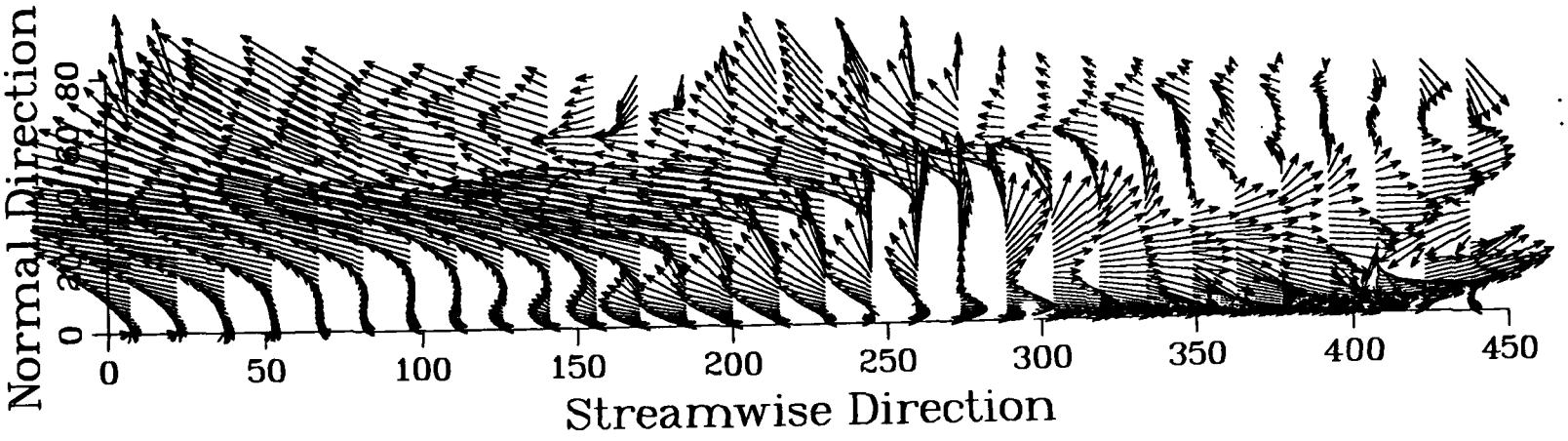

Figure 21: Streamwise-Normal View of an Outflow; Right Side

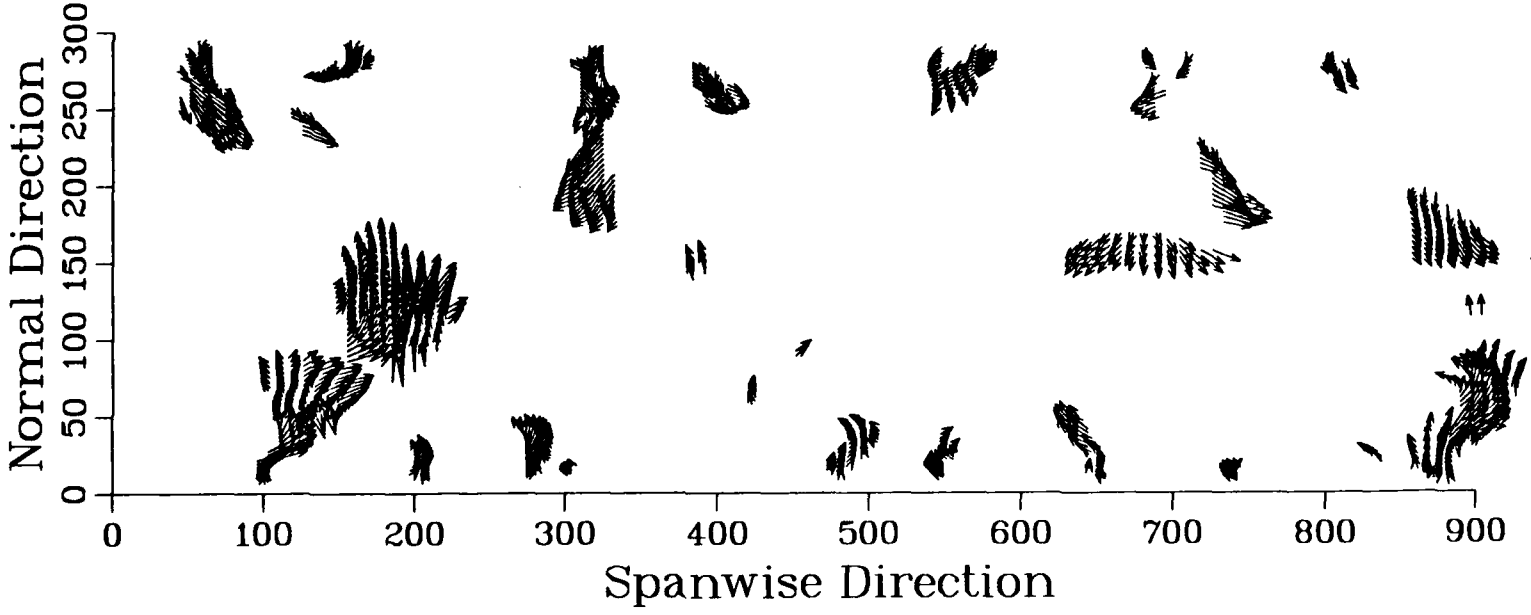

Figure 22: Second Quadrant Reynolds Shear Stress

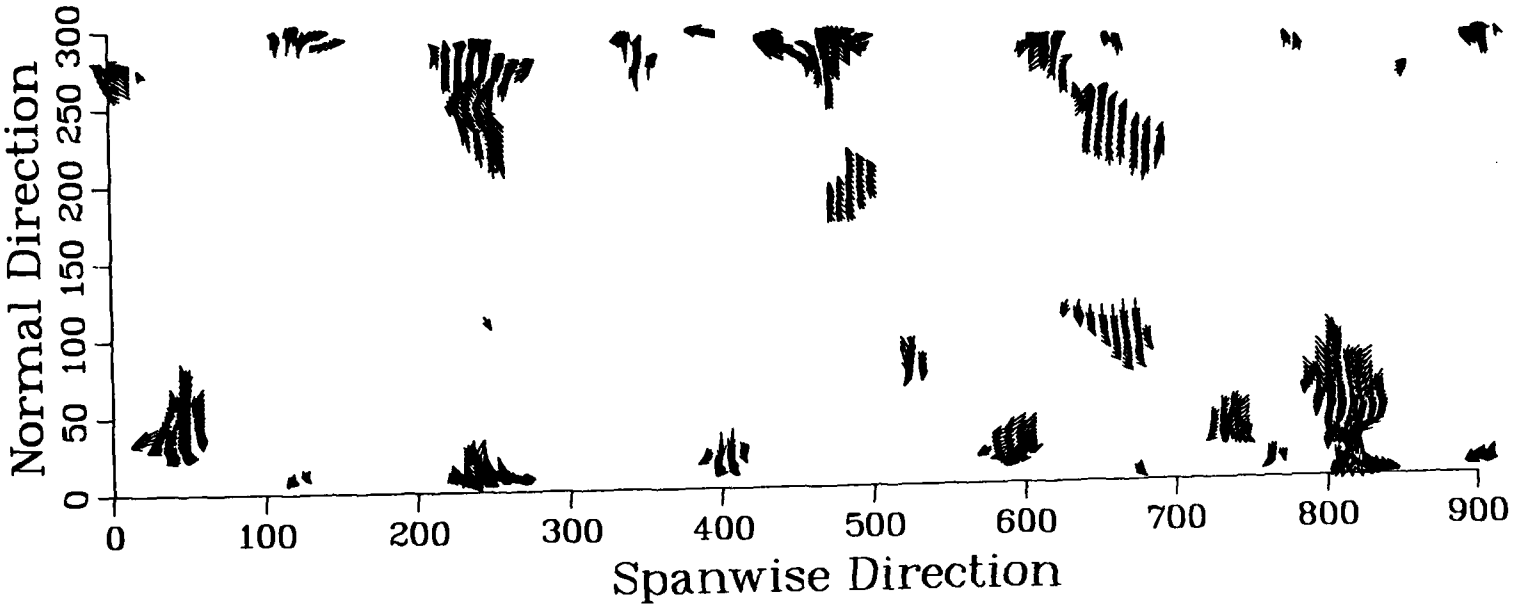

Figure 23: Fourth Quadrant Reynolds Shear Stress

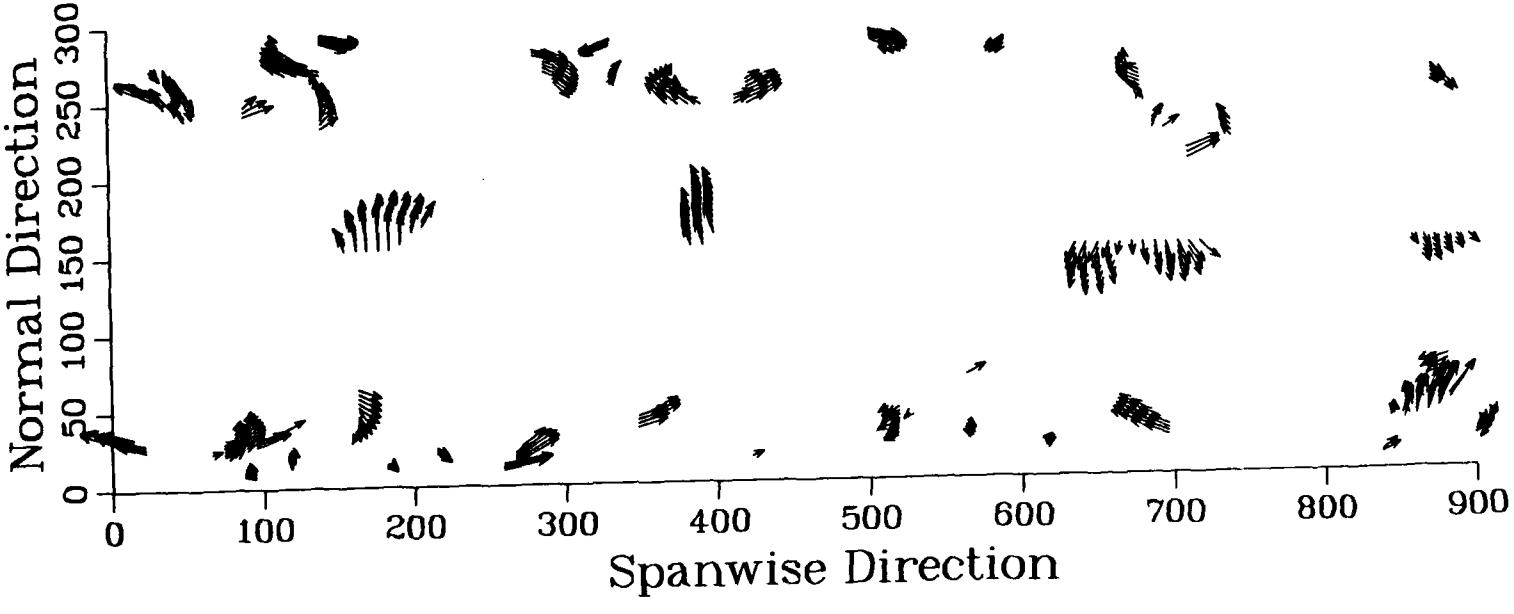

Figure 24: First and Third Quadrant Reynolds Shear Stress

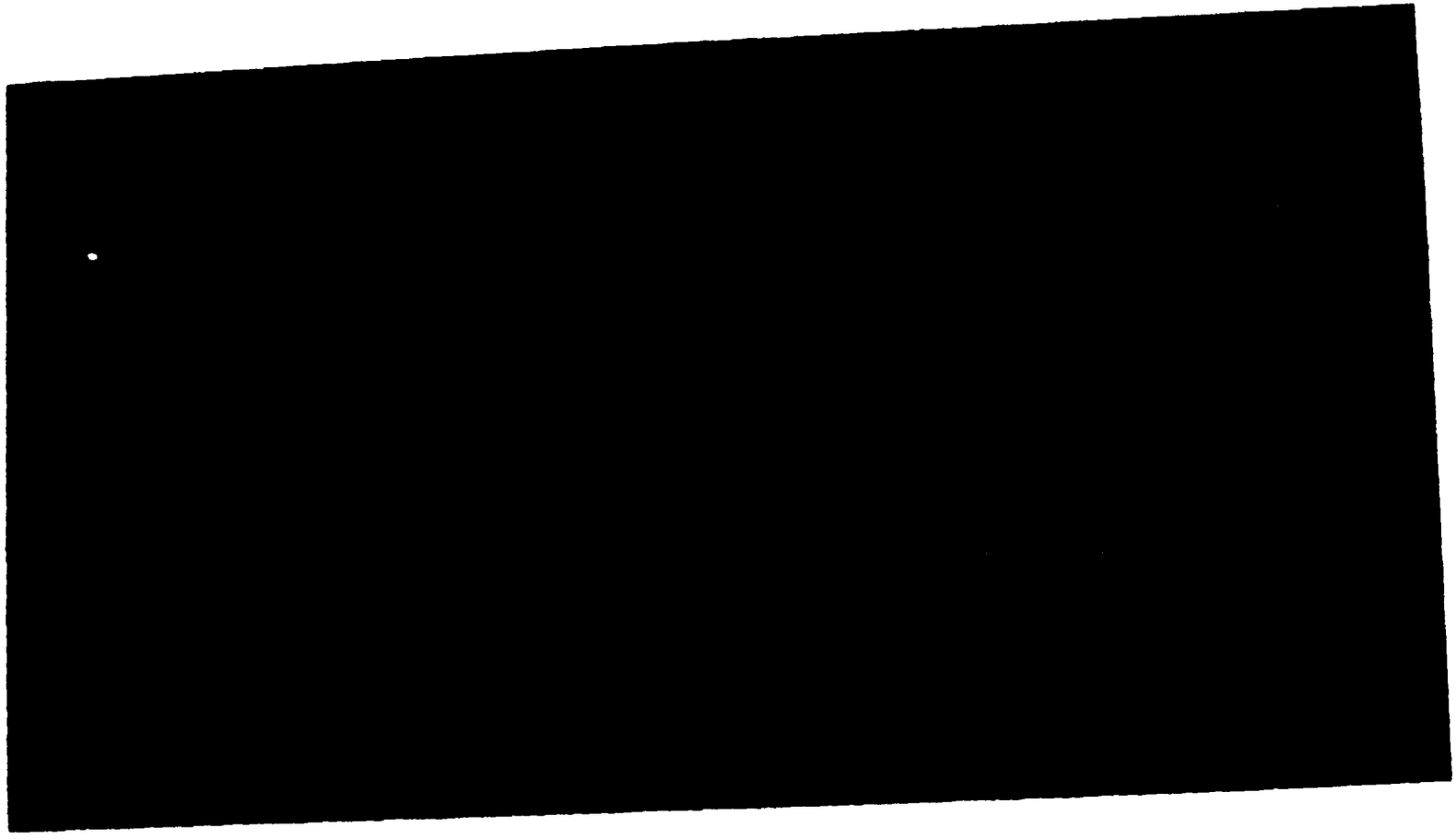

Figure 25: Reynolds Shear Stress, $y^+ = 1.62$

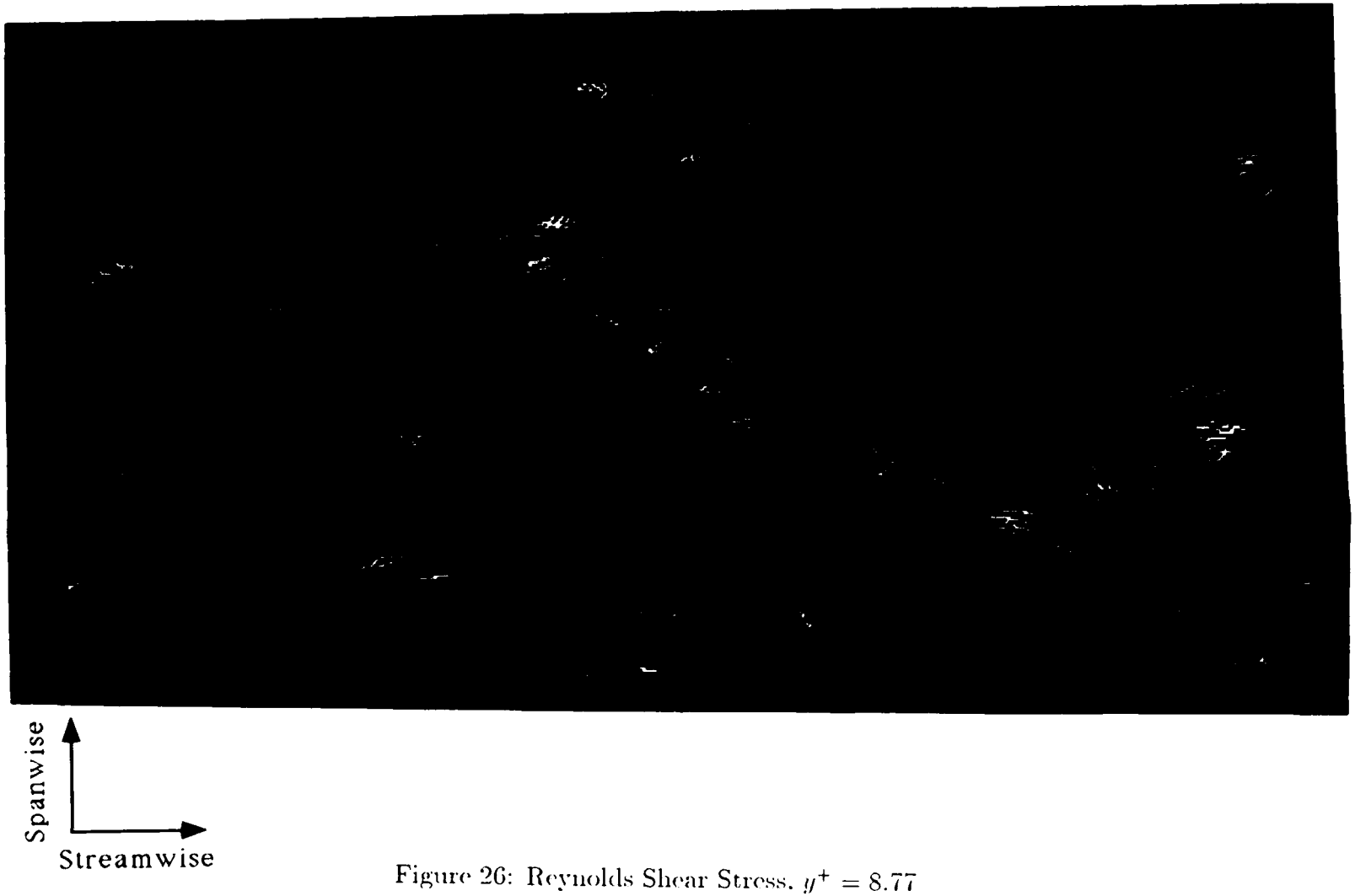

Figure 26: Reynolds Shear Stress, $y^+ = 8.77$

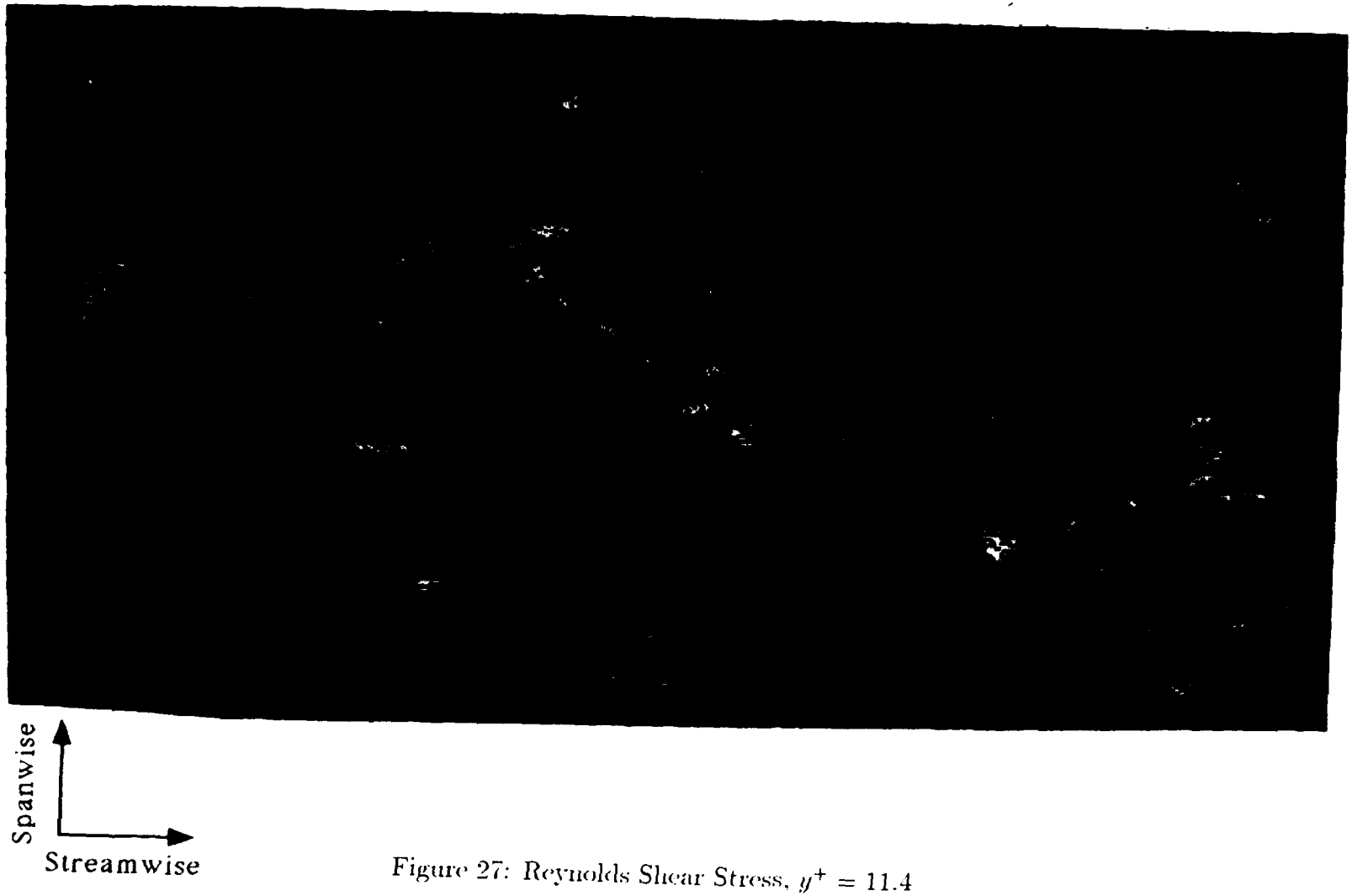

Figure 27: Reynolds Shear Stress, $y^+ = 11.4$

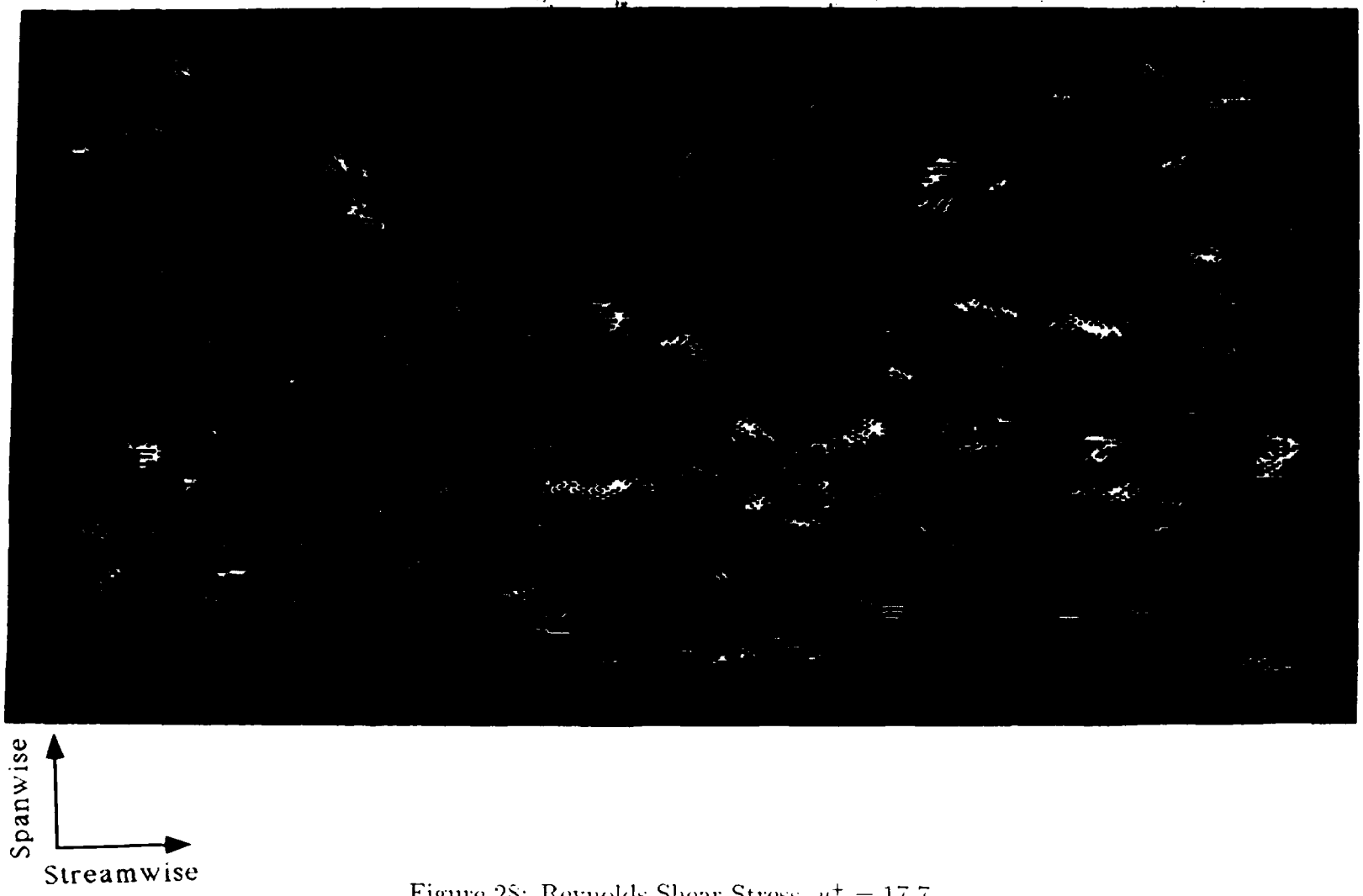

Figure 28: Reynolds Shear Stress, $y^+ = 17.7$

Figure 29: Reynolds Shear Stress, $y^+ = 38.8$

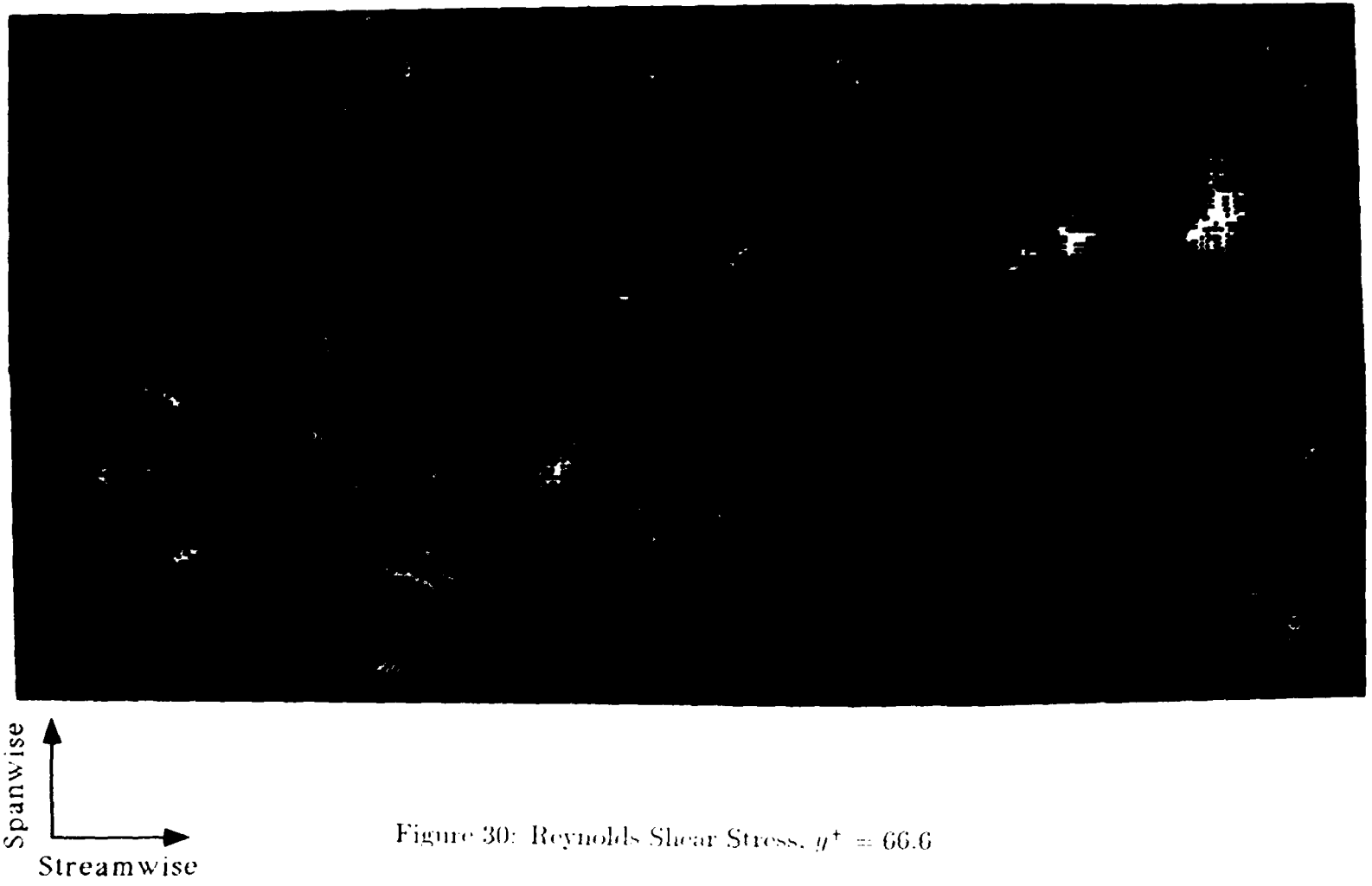

Figure 30: Reynolds Shear Stress, $y^+ = 66.6$

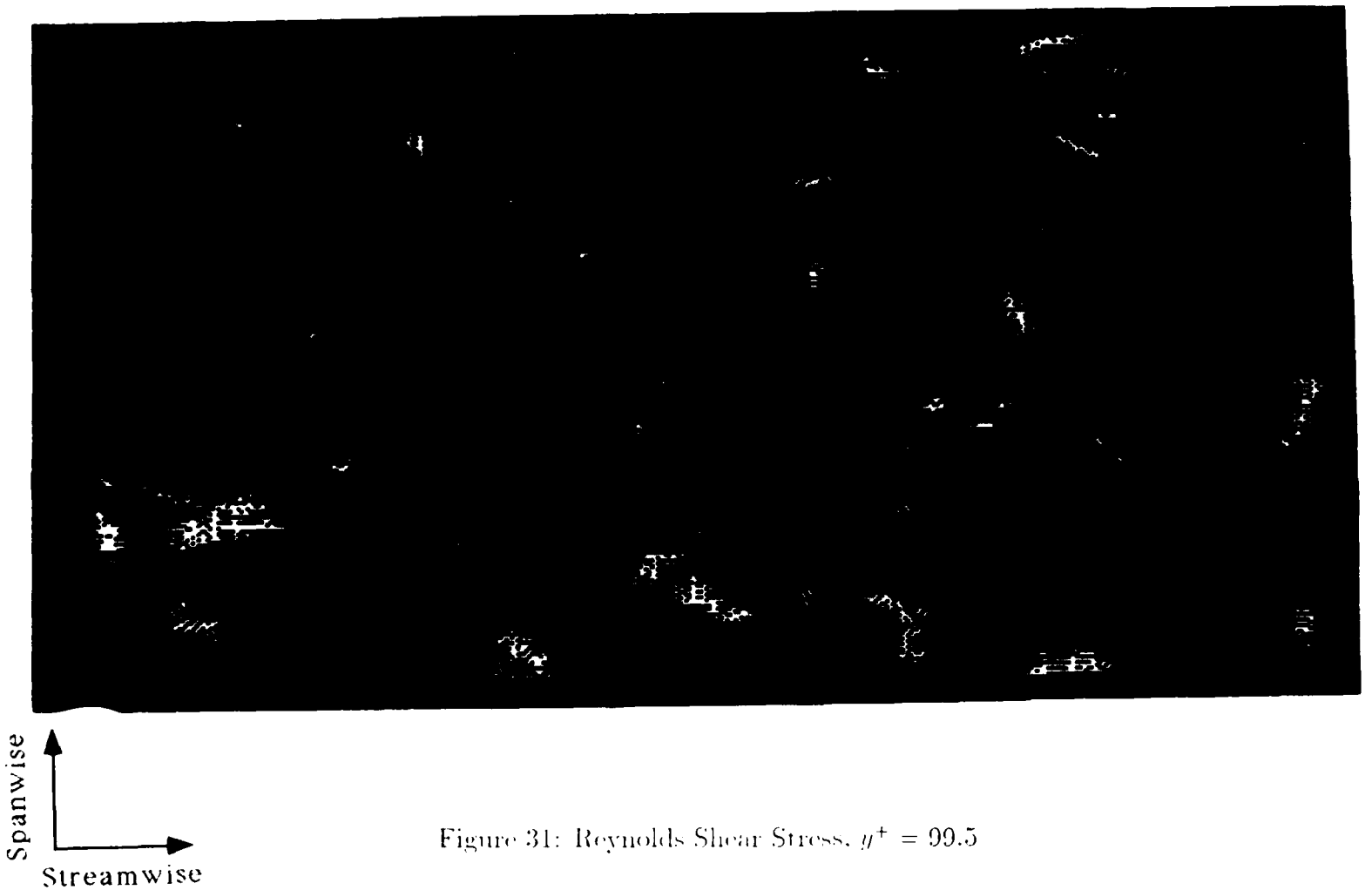

Figure 31: Reynolds Shear Stress, $y^+ = 99.5$

REFERENCES

1. Kuzan, J.D., and Fickie, K.D., "Direct Numerical Simulation of Turbulent Couette Flow," BRL Memorandum Report No. BRL-MR-3848, US Army Ballistic Research Laboratory, Aberdeen Proving Ground, MD, June 1990.

2. Hanratty, T.J., "A Conceptual Model of the Viscous Wall Region," Near Wall Turbulence, Hemisphere Publishing Company, Washington, DC, 1989.

3. Townsend, A.A., The Structure of Turbulent Shear Flow, Cambridge University Press, Cambridge, MA, 1976.

4. Nishino, K., Kasagi, N., and Hirata, M., "Streamwise Pseudo-Vortical Structures and Associated Vorticity in the Near-Wall Region of a Wall-Bounded Turbulence Shear Flow," 9th Symposium on Turbulence, Rolla, MO, 1984.

5. Lyons, S.L., "A Direct Numerical Simulation of Fully Developed Turbulent Channel Flow with Passive Heat Transfer," Ph.D. Thesis, Department of Chemical Engineering, University of Illinois, Urbana, IL, 1989.

INTENTIONALLY LEFT BLANK.

No of Copies	Organization
1	Office of the Secretary of Defense OUSD(A) Director, Live Fire Testing ATTN: James F. O'Bryon Washington, DC 20301-3110
2	Administrator Defense Technical Info Center ATTN: DTIC-DDA Cameron Station Alexandria, VA 22304-6145
1	HQDA (SARD-TR) WASH DC 20310-0001
1	Commander US Army Materiel Command ATTN: AMCDRA-ST 5001 Eisenhower Avenue Alexandria, VA 22333-0001
1	Commander US Army Laboratory Command ATTN: AMSLC-DL Adelphi, MD 20783-1145
2	Commander US Army, ARDEC ATTN: SMCAR-IMI-I Picatinny Arsenal, NJ 07806-5000
2	Commander US Army, ARDEC ATTN: SMCAR-TDC Picatinny Arsenal, NJ 07806-5000
1	Director Benet Weapons Laboratory US Army, ARDEC ATTN: SMCAR-CCB-TL Watervliet, NY 12189-4050
1	Commander US Army Armament, Munitions and Chemical Command ATTN: SMCAR-ESP-L Rock Island, IL 61299-5000
1	Commander US Army Aviation Systems Command ATTN: AMSAV-DACL 4300 Goodfellow Blvd. St. Louis, MO 63120-1798

No of Copies	Organization
1	Director US Army Aviation Research and Technology Activity ATTN: SAVRT-R (Library) M/S 219-3 Ames Research Center Moffett Field, CA 94035-1000
1	Commander US Army Missile Command ATTN: AMSMI-RD-CS-R (DOC) Redstone Arsenal, AL 35898-5010
1	Commander US Army Tank-Automotive Command ATTN: AMSTA-TSL (Technical Library) Warren, MI 48397-5000
1	Director US Army TRADOC Analysis Command ATTN: ATAA-SL White Sands Missile Range, NM 88002-5502
(Class. only) 1	Commandant US Army Infantry School ATTN: ATSH-CD (Security Mgr.) Fort Benning, GA 31905-5660
(Unclass. only) 1	Commandant US Army Infantry School ATTN: ATSH-CD-CSO-OR Fort Benning, GA 31905-5660
1	Air Force Armament Laboratory ATTN: AFATL/DLODL Eglin AFB, FL 32542-5000
	Aberdeen Proving Ground
2	Dir, USAMSAA ATTN: AMXSY-D AMXSY-MP, H. Cohen
1	Cdr, USATECOM ATTN: AMSTE-TD
3	Cdr, CRDEC, AMCCOM ATTN: SMCCR-RSP-A SMCCR-MU SMCCR-MSI
1	Dir, VLAMO ATTN: AMSLC-VL-D

No. of Copies	Organization
2	Commander US Army, ARDEC ATTN: SMCAR-AET-A, R. Kline H. Hudgins Picatinny Arsenal, NJ 07806-5000
1	Commander US Army Missile Command ATTN: AMSMI-RDK (W. Dahlke) Redstone Arsenal, AL 35898-5010
1	Commander Naval Surface Warfare Center ATTN: Dr. W. Yanta Aerodynamics Branch K-24, Bldg. 402-12 Silver Spring, MD 20910
1	Georgia Institute of Technology The George W. Woodruff School of Mechanical Engineering ATTN: Dr. G.P. Neitzel Atlanta, GA 30332-0405

No. of Copies Organization

USER EVALUATION SHEET/CHANGE OF ADDRESS

This Laboratory undertakes a continuing effort to improve the quality of the reports it publishes. Your comments/answers to the items/questions below will aid us in our efforts.

1. BRL Report Number BRL-MR-3857 Date of Report AUGUST 1990

2. Date Report Received _____

3. Does this report satisfy a need? (Comment on purpose, related project, or other area of interest for which the report will be used.) _____

4. Specifically, how is the report being used? (Information source, design data, procedure, source of ideas, etc.) _____

5. Has the information in this report led to any quantitative savings as far as man-hours or dollars saved, operating costs avoided, or efficiencies achieved, etc? If so, please elaborate. _____

6. General Comments. What do you think should be changed to improve future reports? (Indicate changes to organization, technical content, format, etc.) _____

CURRENT ADDRESS

Name

Organization

Address

City, State, Zip Code

7. If indicating a Change of Address or Address Correction, please provide the New or Correct Address in Block 6 above and the Old or Incorrect address below.

OLD ADDRESS

Name

Organization

Address

City, State, Zip Code

(Remove this sheet, fold as indicated, staple or tape closed, and mail.)